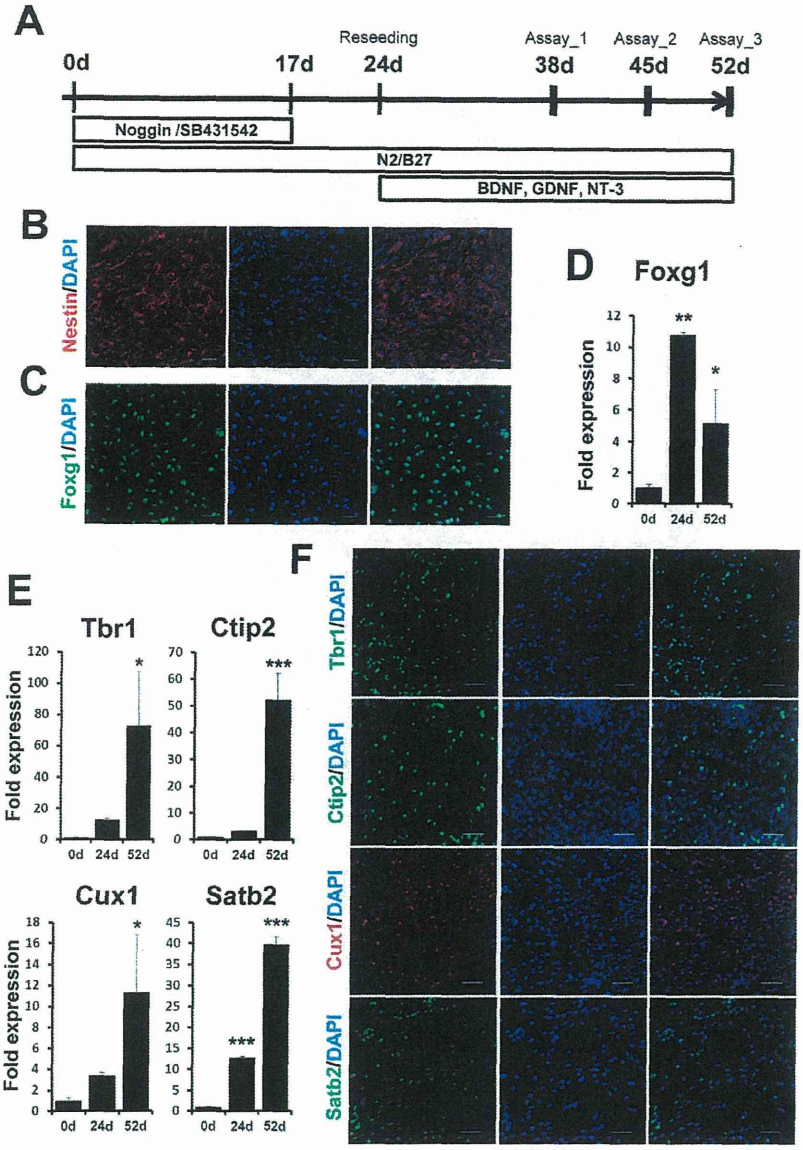

Figure 1. Differentiation of forebrain neurons from hiPS cells. (A) Experimental scheme of neural differentiation from hiPS cells, 253G4. Nestin-positive neuroepithelial cells (B) and Foxg1-positive cells (C) were observed at days 17 and 24, respectively. Scale bar, 50 μm. Expression levels of *Foxg1* (D) and the neocortical markers *Tbr1*, *Ctip2*, *Cux1*, and *Satb2* (E) at days 0, 24, and 52. Expression levels were measured by qPCR and normalized by that of GAPDH. "Fold expression" is shown as a ratio of day 24/day 0 or day52/day 0. Each column represents the mean ± SD of 3 assays. $^{*}p<0.05$, $^{**}p<0.01$, $^{***}p<0.001$, significantly different from day 0 by Dunnett's test. (F) ICC staining of Tbr1-, Ctip2-, Cux1- and Satb2-positive cells at day 52. Scale bar, 50 μm.
doi:10.1371/journal.pone.0025788.g001

western blotting, but their expression levels did not change markedly over time (Figure 4A, C). Aph-1 has two isoforms in human, Aph-1A and Aph-1B, which are considered to have different effects on the production of Aβ species related to AD [24]. Their expression levels measured by qPCR were relatively constant (Figure 4D). The Aph-1B/Aph-1A ratios also did not show significant differences among the time points analyzed here (Figure 4E).

Aβ has several species, including Aβ40 and Aβ42, which have emerged as two of the most robust Aβ measurements in brain. Recent studies suggest that Aβ40 and Aβ42 may have different effects on Aβ aggregation or oligomerization [25,26]. We measured Aβ40 and Aβ42 secreted into conditioned media for 2 days by sandwich ELISA. Both types of Aβ increased with time (Figure 5A). The level of Aβ40 was higher than that of Aβ42, compatible with previous reports [4,27,28,29,30]. Interestingly, the ratio of Aβ42/Aβ40 was highest at day 38, and there was no significant difference between days 45 and 52 (Figure 5B).

Inhibition of Aβ40 and Aβ42 secretion

We examined whether the differentiated neurons contained funtional β- and γ-secretases and whether Aβ secretion could be controlled. We selected the most effective, commercially available β- and γ-secretase inhibitors, β-secretase inhibitor IV (BSI) [31]

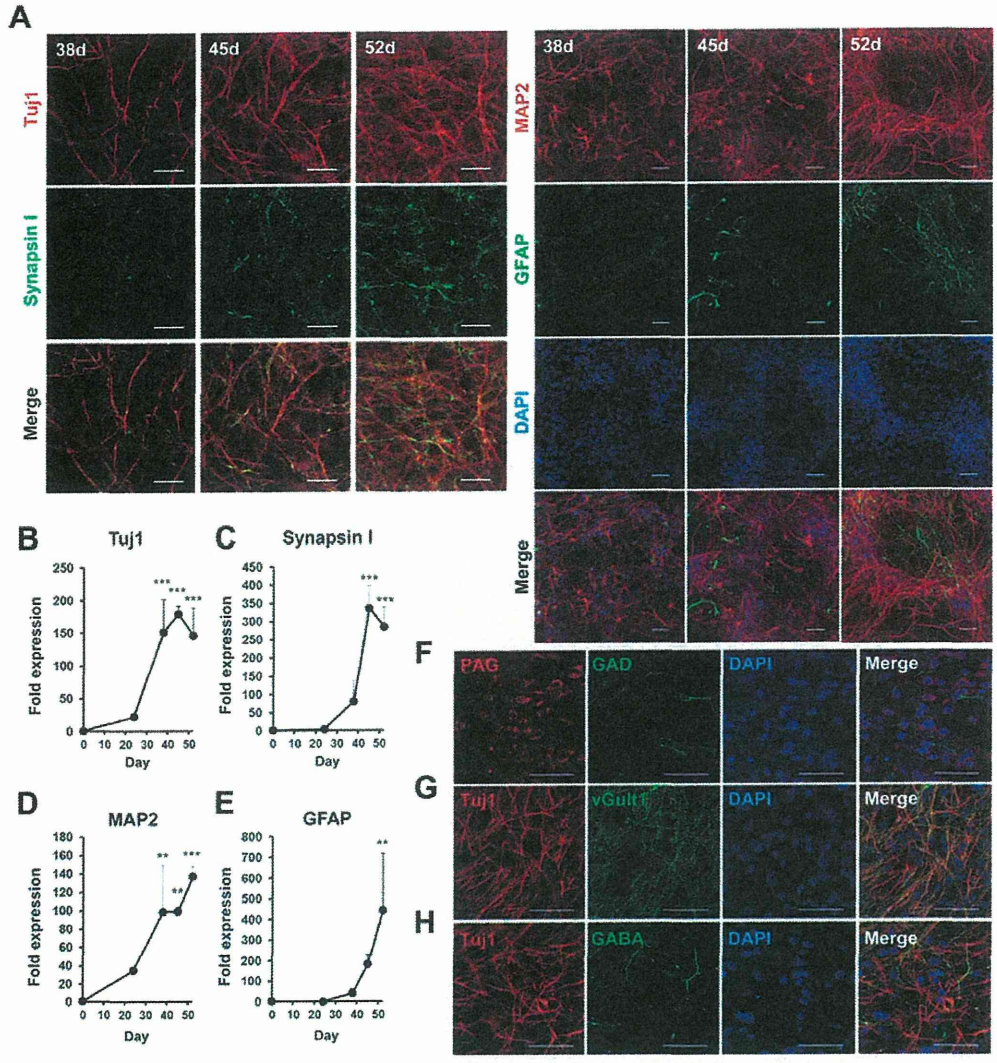

Figure 2. Characterization of neuronal and glial cells differentiated from hiPS cells. (A) Time-dependent morphological changes of cells reseeded in a 24-well plate. Neuronal and glial cells were stained by anti-Tuj1 (left; red), anti-synapsin I (left; green), anti-MAP2 (right; red), and anti-GFAP (right; green) antibodies and DAPI (right; blue) at 38, 45, and 52 days. Scale bar, left; 20 μm, right; 50 μm. Expression levels of Tuj1 (B), synapsin I (C), MAP2 (D), and GFAP (E) at days 0, 24, 38, 45, and 52 were measured by qPCR and normalized by that of GAPDH. "Fold expression" is the ratio of expression at each day compared to day 0. Each point represents mean ± SD of 3 assays. $^{*}p<0.05$, $^{**}p<0.01$, $^{***}p<0.001$, significantly different from day 0 by Dunnett's test. (F–H) Neurotransmitter phenotypes at day 52. PAG (red)- and GAD (green)-positive (F), vGlut1 (green)- and Tuj1 (red)-positive (G), and GABA (green)- and Tuj1 (red)-positive cells (H). Blue, DAPI. Scale bar, 50 μm.
doi:10.1371/journal.pone.0025788.g002

and γ-secretase inhibitor XXI/Compound E (GSI) [32], respectively. We also examined the effect of a non-steroidal anti-inflammatory drug (NSAID), sulindac sulfide [33], because some NSAIDs directly modulate γ-secretase activity to selectively lower Aβ42 levels [33,34]. The cells were treated with each drug for 2 days, and Aβ was monitored in the collected media at day 38 or 52.

There were different susceptibilities to all three drugs between days 38 and 52 (Figure 6) as revealed by two-way analysis of variance (ANOVA) [significant interaction between day and dose (BSI, $p<0.001$ in Aβ40 and Aβ42, respectively; GSI, $p<0.001$ in Aβ40 and Aβ42, respectively; NSAID, $p<0.001$ in Aβ42)]. Following BSI and NSAID treatment, secretion of Aβ40 and Aβ42 was decreased in a dose-dependent manner (Figure 6A, B, E, and F). NSAID especially showed more efficient inhibition of Aβ42 than that of Aβ40, consistent with a previous report [33]. Following GSI treatment (Figure 6C, D), secretion of both Aβ40 and Aβ42 was increased at lower doses (10^{-11}–10^{-8} M), but was inhibited at higher doses (10^{-7}–10^{-6} M) at day 52. This phenomenon, which is called a "gradual Aβ rise", was observed following the addition of other GSIs in a cell line system [35]. On the other hand, secretion of both Aβ40 and Aβ42 at day 38 showed a fast increase at lower doses (10^{-11}–10^{-9} M) (Aβ surge) and drastic decline at 10^{-8} M. We also examined the effects of these inhibitors on cell viability using the lactate dehydrogenase (LDH) assay. Two-day-treatments with the highest concentrations

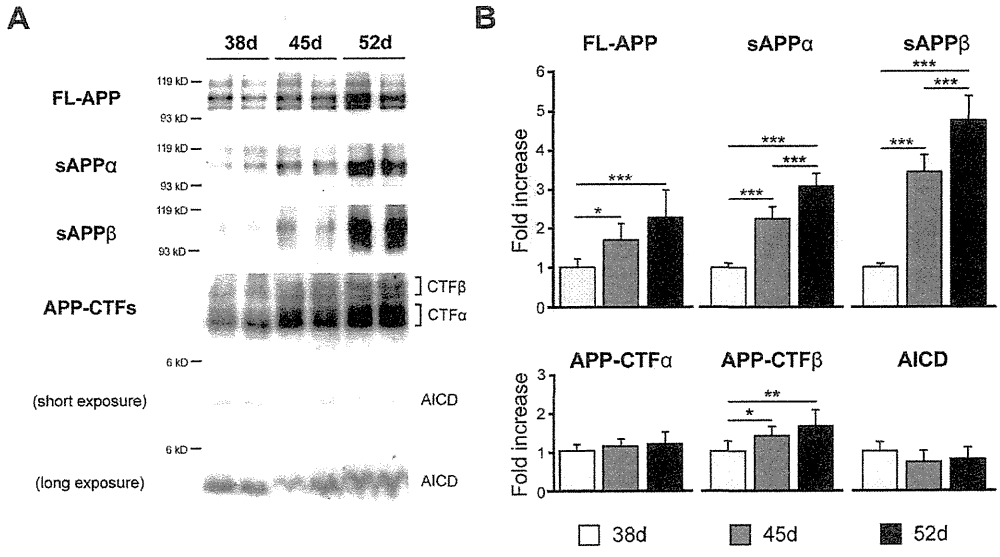

Figure 3. APP was expressed in hiPS cell-derived neuronal cells. HiPS cell-derived neuronal cells express full-length APP, sAPPα, sAPPβ, APP-CTFα, APP-CTFβ and AICD at 38, 45, and 52 days. (A) Representative western blots of APP and its fragments. (B) Each column represents mean ± SD of 8 samples measured by quantitative western blot analysis and normalized by that of β-actin. "Fold expression" represents the ratio of expression on the given day compared to day 38. $^{*}p<0.05$, $^{**}p<0.01$, $^{***}p<0.001$, Tukey's test.
doi:10.1371/journal.pone.0025788.g003

of BSI, GSI, or NSAID did not induce cell death (Table S1). We also traced these experiments using human ES (hES) cell (H9)-derived neuronal cells (Figure S4) because remaining expression of reprogramming factors, Oct3/4 and Klf4, were observed in hiPS cell (253G4)-derived neuronal cells (Figure S6). The Aβ production and its inhibition by these drugs in hES cell-derived neuronal cells were relatively similar to those in hiPS cell-derived ones (Figure S5). These data showed that BSI, GSI, and NSAID partially or fully blocked Aβ production in the hiPS cell-derived neuronal cells, indicating that these cells expressed functional β- and γ-secretases.

Discussion

AD is the most common cause of dementia in the elderly, with progressive neuronal loss in the cerebral cortex and hippocampal formation. Although the underlying etiology of most AD remains unclear, Aβ is thought to play a pivotal role in its pathogenesis. Studies from animal and cellular models have shown that mutations in the APP, PS1, and PS2 genes affected the production of Aβ, which contributes to the formation of amyloid plaques [19]. In several strains of mouse models, Aβ levels in brain tissue, cerebrospinal fluid (CSF), and plasma have been associated with AD pathogenesis and cognitive impairment [27,28,36]. Human samples from clinical AD patients have also been used for pathological and biochemical analyses to understand the etiology of AD. Aβ levels in CSF and plasma have been examined to evaluate their risks for AD [29,37], but brain tissues are only available postmortem for such analyses. On the other hand, immortalized human cell lines derived from kidney or brain, primary neurons derived from mice and rats, or cells artificially overexpressing APP or presenilin with or without familial AD mutations have been utilized for *in vitro* studies [4,30]. There is no doubt that these cells are quite different from living neurons in the human body in terms of innate qualities. Although we have had no choice until recently, important advances in technology of iPS cells may now provide the opportunity to use intact human-derived neuronal cells [38].

We evaluated whether iPS cell-derived neuronal cells could be applied to an *in vitro* cell-based assay system for AD research. In particular, further investigations into the metabolic mechanisms of Aβ are requisite for drug development to treat the brains of patients afflicted with AD. In this respect, we provide a profile of the molecular components associated with Aβ production in hiPS cell-derived neuronal cells and propose to add an Aβ assay system using these cells to the panel of generalized Aβ-monitoring systems (Table 1). Human neuronal cells are considered to provide more accurate human neuronal conditions within which to evaluate drug efficacy or toxicity than other human cell lines (e.g., cancer lines). Furthermore, we would be able to investigate how hiPS cell-derived neuronal cells reflect AD-related physiological and pathological conditions based on Aβ production.

In the present study, we characterized iPS cell-derived neuronal cells in terms of their expression of neuronal and glial markers by exposing them to Noggin and SB431542 during their differentiation (Figures 1 and 2). We observed increases in GFAP mRNA levels and in synapsin I-positive synaptic puncta at day 52. This was consistent with data showing that the existence of astrocytes promotes synaptic activity in human ES cell-derived neurons [40]. When differentiation occurred in the presence of non-morphogens, we obtained mainly glutamatergic neurons (Figure 2F, G), quite in line with previous reports of concerning hES and hiPS cells [10,11]. Expression of the forebrain marker Foxg1 suggests a default forebrain identity of the 253G4 iPS cells used in this study (Figure 1C, D). We also observed the expression of the neocortex-specific transcriptional factors Tbr1, Ctip2, Cux1, and Satb2 (Figure 1E, F). These expression schemes appear to mimic human neocortical development *in vitro* [16], although further analyses are needed to assist in understanding human neuronal subtype-specific differentiation.

This is the first study to observe the expression of APP, β- and γ-secretase, and the production of Aβ in hiPS cell-derived neuronal

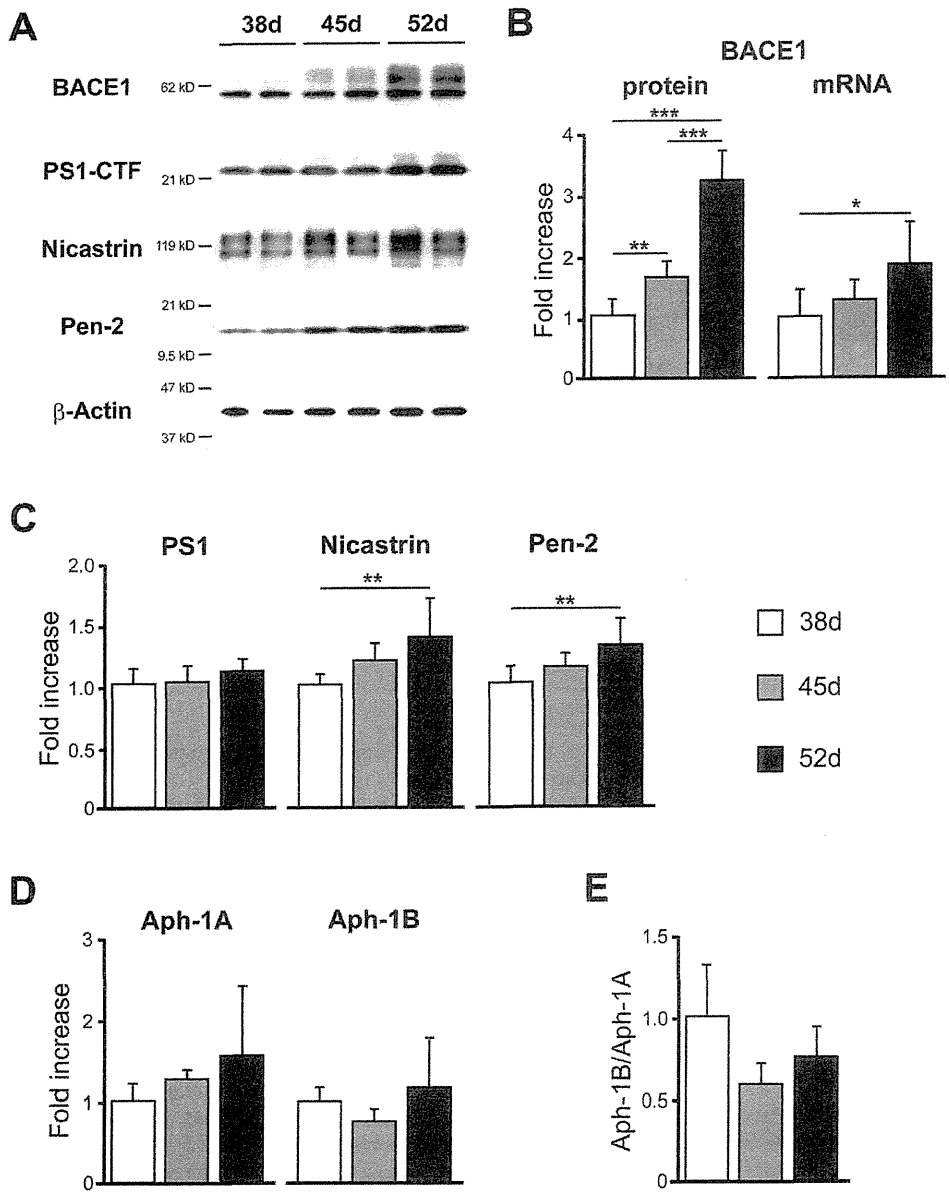

Figure 4. β-Secretase and γ-secretase components were expressed in hiPS cell-derived neuronal cells. The hiPS cell-derived neuronal cells express BACE1 protein and mRNA (B), γ-secretase components; presenilin 1(PS1), nicastrin, Pen-2 (C), and Aph-1A, and Aph-1B (D) at days 38, 45, and 52. Expression levels were quantified by western blot analysis (n = 8) (B, C) or qPCR (n = 3) (D) and normalized by that of β-actin. "Fold expression" represents the ratio of expression on the given day compared to day 38. (E) The ratio Aph-1B/Aph-1A. Data represent mean ± SD. (A) Representative western blots of BACE1 and γ-secretase components at 38, 45, and 52 days. $^{*}p<0.05$, $^{**}p<0.01$, $^{***}p<0.001$, Tukey's test.
doi:10.1371/journal.pone.0025788.g004

cells. APP, sAPPβ, APP-CTFβ and BACE1 protein levels were increased (Figures 3 and 4), but protein levels of γ-secretase components were not significantly different during the period from day 38 to 52 (Figure 4C, D). Aβ production in hiPS cell 253G4-derived neuronal cells increased with differentiation course (Figure 5A), however that in another hiPS cell 201B7 [5]- and in hES H9-derived neuronal cells did not increase (Figures S5 and S7) although all cell lines showed development of synapse (Figure S4A) as Aβ releasing site [41], indicating that besides synaptogenesis, subtle changes in localization and assembly of APP [42], BACE1, γ-secretase components would be critical for Aβ production.

The Aβ42/Aβ40 ratio unexpectedly showed a significant decrease from day 38 to 45 (Figure 5B). Serneels *et al.* reported that the γ-secretase complex containing Aph-1B was active and involved in the generation of amyloidogenic Aβ42 [24]. Our data showed that the Aph-1B/Aph-1A ratio did not change significantly with cell differentiation (Figure 4E); therefore, the Aβ42/Aβ40 ratio may be influenced by other unknown factors interacting directly or indirectly with γ-secretase.

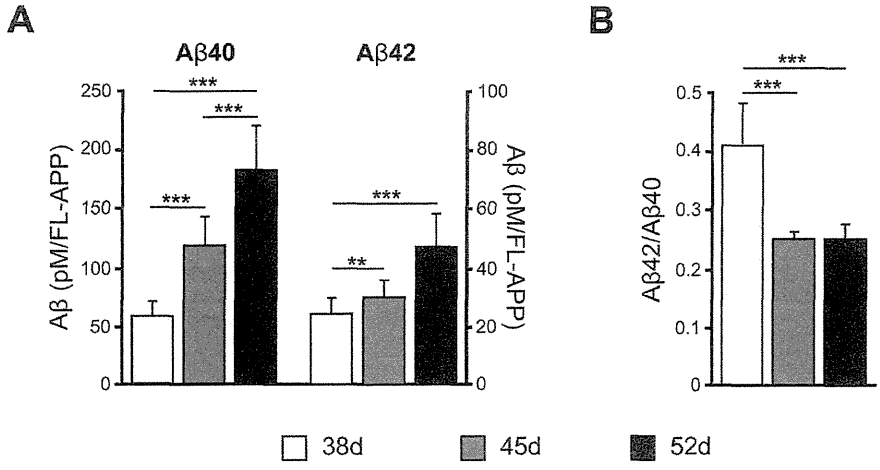

Figure 5. Aβ was produced in hiPS cell-derived neuronal cells. (A) Aβ40 or Aβ42 secreted into the conditioned media and FL-APP were measured by sandwich ELISA and western blot analysis, respectively. Expression level of Aβ was normalized by that of FL-APP. (B) Aβ42/Aβ40 ratios. Data represent the mean ± SD of 8 assays. *, $^{\#}p<0.05$, **, $^{\#\#}p<0.01$, ***, $^{\#\#\#}p<0.001$, Tukey's test.
doi:10.1371/journal.pone.0025788.g005

BSI, GSI, and the NSAID sulindac sulfide inhibited Aβ production in this human neuronal cell system (Figure 6). The inhibitory effect on Aβ production by GSI showed a characteristic difference between days 38 (Aβ surge) and 52 (gradual Aβ rise) (Figure 6C, D). Aβ surge at day 38 was also observed in another hiPS cell (201B7)-derived neuronal cells (Figure S7) as well as in hES cell line, H9-derived ones (Figure S5). At day 38, GSI might promote neuronal differentiation with synaptogenesis via blocking Notch signaling [43] rather than inhibition of Aβ production, leading to Aβ surge. Another possible explanation for Aβ surge is that change in conformation or components of the γ-secretase affects the sensitivity of γ-secretase to GSI (total Aβ, Aβ40, Aβ42, and Aβ42/Aβ40), although levels of mRNA and the ration for Aph-1A and Aph-1B do not change between days 38 and 52 (Figure 4D, E) Thus, for precise Aβ monitoring in human stem cell-derived neuronal cells, it is necessary to use neuronal cells with a sufficient substrate level and synaptogenesis, because Aβ is released presynaptically, as mentioned above.

Some NSAIDs are known to preferentially lower Aβ42 [33,34]. Our data showed that sulindac sulfide was capable of inhibiting Aβ42 secretion at high concentrations ($\geq 10^{-5}$ M) (Figure 6F), although a few NSAIDs do not show therapeutic effects for AD. Negative results might be due to low γ-secretase modulator potency [44]. To discover novel effective drugs for modulating β- or γ-secretase activity, the *in vitro* hiPS cell-derived neuronal cell assay system might be expected to yield such drugs.

Familial AD patient specific neuronal cells generated by direct conversion (induced neuron, iN) show higher Aβ42/Aβ40 ratio than those of unaffected individuals [45]. Based on this report, hiPS/hES cell-derived neurons expressing mutant PS1, PS2, or APP may show higher Aβ42/Aβ40 ratio. Comparing to our results, the levels of Aβs in this assay (Aβ40; ~1.7 ng/ml at day 52) is higher than that using iN cells (Aβ40; ~0.1 ng/ml), although iN cells become functional neurons more quickly. The optimization of neuronal cell condition for comparison of the Aβ42/Aβ40 ratio between multiple iPS cell-derived neuronal cells may be required.

In conclusion, our findings indicate that hiPS cell-derived neuronal cells express functional β- and γ-secretases related to the production of Aβ in the present experimental conditions. In addition, our data provide the proof in principle that hiPS cell-derived neuronal cells can be applied to drug screening and AD patient-specific iPS cell research.

Materials and Methods

Antibodies and reagents

Primary antibodies used were as follows: mouse anti-Nestin (1:200, Millipore, Temecula, CA), mouse anti-Tuj1 (1:2000, Covance, Princeton, NJ), rabbit anti-GFAP (1:500, DAKO, Carpinteria, CA), rabbit anti-Synapsin I (1:500, Millipore), mouse anti-Cux1 (1:100, Abnova, Taipei, Taiwan), rabbit anti-Satb2 (1:1000, Abcam, Cambridge, UK), rat anti-Ctip2 (1:500, Abcam), rabbit anti-Tbr1 (1:500, Abcam), rabbit anti-vGlut1 (1:1000, Synaptic Systems, Göttingen, Germany), rabbit anti-Foxg1 (1:100, Abcam), rabbit anti-GABA (1:1000, Sigma-Aldrich, St. Louis, MO), rabbit anti-GAD65/67 (1:200, Millipore), mouse anti-PAG [46] (1:500), rabbit anti-APP (1:15000, Sigma-Aldrich), mouse anti-APP (1 μg/ml, Millipore), rabbit-anti BACE (1:2000, Merck, Darmstadt, Germany) mouse anti-PS1 loop C-terminus (1:1000, Millipore), rabbit anti-nicastrin (1 μg/ml, Thermo Scientific, Rockford, IL), rabbit anti-Pen-2 (1:1000, Invitrogen, San Diego, CA), mouse anti-MAP2 (1:200, Millipore), goat anti-ChAT (1:100, Millipore), guinea pig anti-VAChT (1:500, Millipore), and mouse anti-β-actin (1:15000, Sigma-Aldrich). We raised rabbit polyclonal antibodies against the carboxyl terminals of human sAPPα (hsAPPα) and sAPPβ using the KLH-conjugated synthetic peptides CRHDSGYEVHHQK and CKTEEISEVKM, respectively (Figure S3). All animal experiments were performed in compliance with the institutional guidelines at RIKEN Brain Science Institute, and were approved by the Animal Care and Use Committee (Permit number: H17-2B031). Each antibody was purified with a peptide-conjugated column [47]. Alexa Fluor 488 and Alexa Fluor 594-conjugated secondary antibodies (Invitrogen) were used for immunofluorescence.

The β-secretase inhibitor IV [31] and γ-secretase inhibitor XXI/Compound E [32] were purchased from Merck. Sulindac sulfide (NSAID) was purchased from Sigma-Aldrich.

Immunocytochemistry

Cells were fixed with 4% paraformaldehyde in phosphate buffered saline (PBS) for 30 min, and incubated in PBS

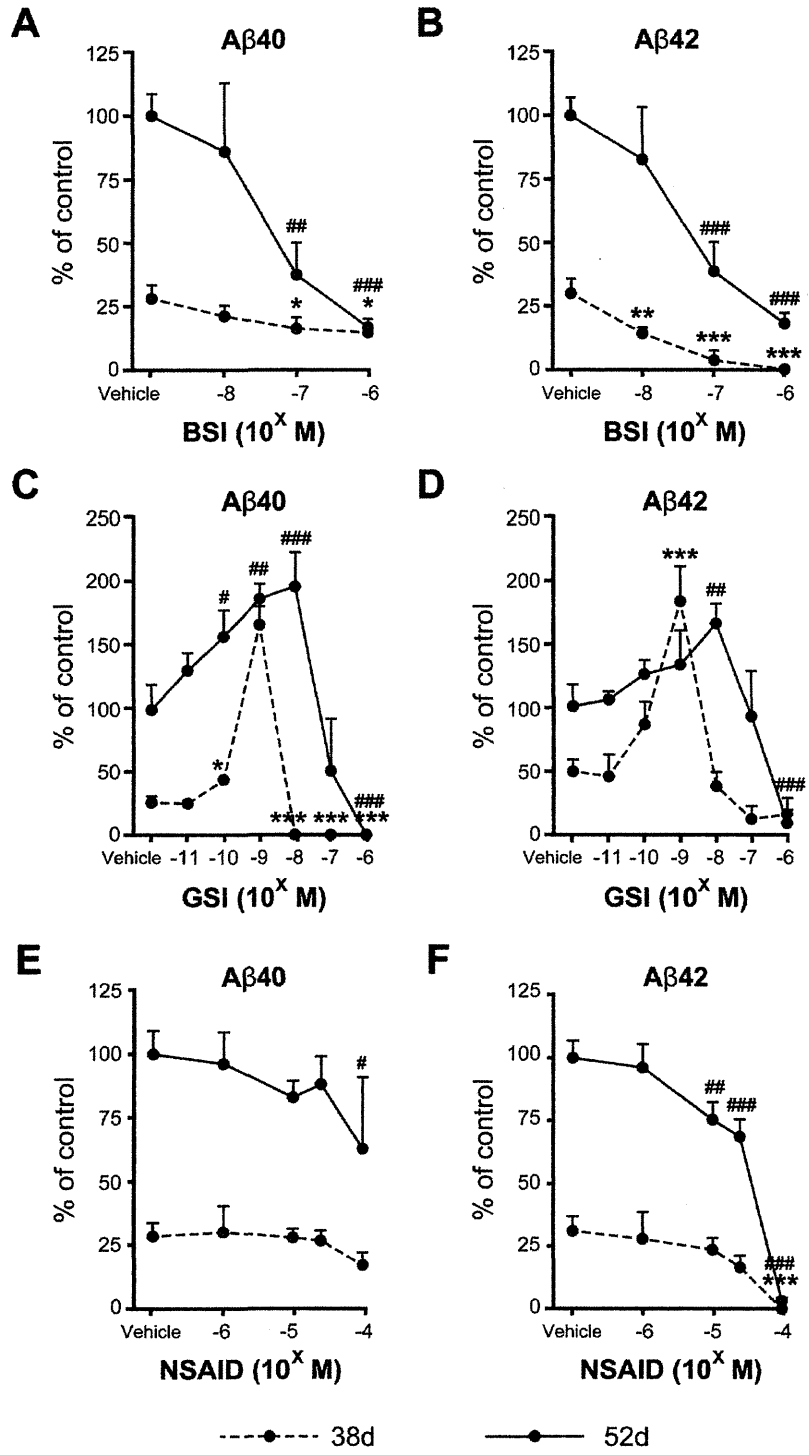

Figure 6. Aβ production was modulated by β- and γ-secretase inhibitors and an NSAID. β-Secretase inhibitor (BSI) (A, B), γ-secretase inhibitor (GSI) (C, D), and NSAID (E, F) were added into hiPS cell-derived neuronal cell cultures at day 36 (dotted line) and 50 (bold line), and two days later amounts of Aβ40 and Aβ42 secreted into the conditioned media were measured. The ratios Aβ40/FL-APP and Aβ42/FL-APP are expressed as percentages of the vehicle-treated group at day 52 and represent mean ± SD of 3 assays. A, B: There were significant main effects of day ($F(1, 16) = 72.5$ and 162.4, $p<0.001$ in Aβ40 and Aβ42, respectively) and dose ($F(3, 16) = 23.1$ and 45.7, $p<0.001$ in Aβ40 and Aβ42, respectively), and significant interaction between day and dose ($F(3, 16) = 13.0$ and 11.7, $p<0.001$ in Aβ40 and Aβ42, respectively) by 2-way ANOVA. C, D: There were significant main effects of day ($F(1, 28) = 240.5$ and 59.1, $p<0.001$ in Aβ40 and Aβ42, respectively) and dose ($F(6, 28) = 70.8$ and 37.8, $p<0.001$ in Aβ40 and Aβ42, respectively), and significant interaction between day and dose ($F(6, 28) = 23.5$ and 15.1, $p<0.001$ in Aβ40 and Aβ42, respectively) by

2-way ANOVA. E, F: There were significant main effects of day ($F(1, 20) = 196.9$ and 418.0, $p<0.001$ in Aβ40 and Aβ42, respectively) and dose ($F(4, 20) = 4.16$, $p = 0.013$ and $F(4, 20) = 91.9$, $p<0.001$ in Aβ40 and Aβ42, respectively), and significant interaction between day and dose ($F(4, 20) = 25.4$, $p<0.001$ in Aβ42) by 2-way ANOVA. *, $^{\#}p<0.05$, **, $^{\#\#}p<0.01$, ***, $^{\#\#\#}p<0.001$, significantly different from respective vehicle-treated groups by Dunnett's test.
doi:10.1371/journal.pone.0025788.g006

containing 0.2% Triton X-100 for 10 min (permeabilization). After blocking with 2% BSA in PBS, cells were incubated with primary antibody diluted with blocking buffer and then washed with PBS. Finally the cells were incubated with secondary antibodies and mounted using ProLong Gold antifade reagent with DAPI (Invitrogen). The immunoreactive cells were visualized using an LSM 700 Laser Scanning Microscope (Carl Zeiss, Jena, Germany) and a Biorevo BZ-9000 fluorescence microscope (Keyence, Osaka, Japan).

Quantitative real-time RT-PCR

Total RNA was isolated from cells using TRIZOL reagent (Invitrogen). Contaminating DNA was removed using the TURBO DNA-free kit (Ambion, Austin, TX), and cDNA was synthesized using ReverTra Ace-α (Toyobo, Osaka, Japan), according to the manufacturers' protocols. Real-time PCR was performed using the StepOnePlus system (Applied Biosystems) and SYBR green reagent (TAKARA, Shiga, Japan). The primers used are listed in Table S2 in the supporting information.

HiPS cell culture and differentiation into neuronal cells

HiPS cells, 253G4 [14] (passage 20–30) or hES cells, H9 were cultured on mitomycin C-treated mouse embryonic fibroblasts in primate ES medium (ReproCELL, Kanagawa, Japan) supplemented with bFGF (Wako Pure Chemicals, Osaka, Japan). To obtain cortical neurons derived from iPS cells, we partially modified a previous method [12,15]. For neural induction, partially dissociated iPS cell colonies, 40–100 μm in diameter, were selected with Cell Strainer (BD Falcon, BD Bioscience, Bedford, MA) and plated on poly-L-lysine (Sigma-Aldrich)/Laminin (BD Biosciences) (PLL/LM)-coated dishes (P1) in N2B27 neuronal differentiation medium [DMEM/F12 (Invitrogen), Neurobasal (Invitrogen), N2 (Invitrogen), B27 minus vitamin A (Invitrogen), L-Gln (Invitrogen)], supplemented with 100 ng/ml human recombinant Noggin (R&D Systems, Minneapolis, MN) and 1 μM SB431542 (Sigma-Aldrich) for 17 days. At day 10, primary colonies were split into small clumps using 200 U/ml collagenase with $CaCl_2$ and plated into PLL/Entactin-Collagen IV-Laminin (Millipore) (ECL)-coated dishes (P2). At day 17, P2 cells were dissociated using Accutase (Innovative Cell Technologies, San Diego, CA) and cultured on PLL/ECL-coated dishes (P3). Finally, at day 24, cells dissociated with Accutase were passed through a 40-μm cell strainer (BD Biosciences), counted, and cultured on PLL/LM/Fibronectin (Millipore)-coated 24-well plates at 2.5×10^4 cells/well in N2B27 medium supplemented with 10 ng/ml BDNF, GDNF, and NT-3 (R&D Systems). Medium changes for cell culture were carried out once every two or three days until day 52.

Aβ sandwich ELISA

At days 38, 45, and 52, two-day incubated conditioned media were collected from cultured neuronal cells and centrifuged at 4,000 *g* for 10 min. The resultant clear supernatants were subjected to sandwich ELISA (Wako) with a combination of monoclonal antibodies specific to the midportion of Aβ and specific to the C-terminal of Aβ40 or Aβ42, to determine the amounts of secreted Aβ, as described previously [20,28,30]. We also examined the inhibitory effect of each drug on Aβ production. All media were replaced with new media containing each drug and two-day conditioned media were analyzed as mentioned above.

Western blot analysis

Western blot analysis was performed as previously described with minor modification. In addition to conditioned media, cell lysates were also collected, extensively washed with PBS, and lysed

Table 1. Panel of Aβ monitoring systems.

Human sample	**Aβ40**	**Aβ42**	**Ref.**
Brain tissue [AD]	↑ (AD/NC)	↑ (AD/NC)	[39]
CSF [AD]	-	↓ (AD/NC)	[37]
	→ (AD/NC)	↓ (AD/NC)	[29]
Plasma [AD]	↑ (AD/NC)	→ (AD/NC)	[29]
iPS cell-derived neuronal cells	Measurable	Measurable	This report
Mouse model	**Aβ40**	**Aβ42**	**Ref.**
Brain [PDAPP]	↑ (Aging)	↑ (Aging)	[36]
Brain [APP23]	↑ (Tg/non-Tg)	↑ (Tg/non-Tg)	[27]
Brain [Tg2576]	↑ (Aging)	↑ (Aging)	[28]
	↑ (Tg/non-Tg)	↑ (Tg/non-Tg)	
CSF [Tg2576]	↓ (Aging)	↓ (Aging)	[28]
Plasma [Tg2576]	↓ (Aging)	↓ (Aging)	[28]
Cell line	**Aβ40**	**Aβ42**	**Ref.**
[APP_{NL}-H4]	Measurable	Measurable	[30]
[CHO-APP_{NL}/SH-SY5Y-APP]	Measurable	Measurable	[4]

AD, Alzheimer's disease; NC, normal control; Tg, transgenic mouse model.
doi:10.1371/journal.pone.0025788.t001

directly with 1× sample buffer (EzApply; ATTO, Tokyo, Japan). The media or cell lysates were separated by 5–20% gradient or 7.5% [FL-APP] or 10% [β-actin] sodium dodecyl sulfate-polyacrylamide gel electrophoresis (SDS-PAGE) and transferred to polyvinylidene difluoride membranes (Hybond-P; GE Healthcare, Buckinghamshire, UK). The blots were probed with an appropriate primary antibody, followed by HRP-conjugated anti-mouse or anti-rabbit IgG (GE Healthcare). The protein bands were visualized using an enhanced chemiluminescence (ECL) detection method (GE Healthcare), and band intensity was analyzed with a densitometer (LAS-4000; GE Healthcare), using the Science Laboratory 2001 Image Gauge software (Fujifilm, Tokyo, Japan). Immunoreactive protein content in each sample was calculated based on a standard curve constructed with each recombinant protein or one of the samples. Each set of experiments was repeated at least two times to confirm the results. The level of β-actin protein, measured by quantitative western blotting using β-actin antibody, was used as an extraction and loading control.

LDH assay

Cell toxicity assays were performed using a cytotoxicity detection kit (LDH, Roche, Mannheim, Germany) according to the manufacturer's protocol.

Statistical analysis

All data were expressed as mean ± SD. Comparisons of mean among more than three groups were done by one-way or two-way ANOVA, followed by *post-hoc* test (PRISM, GraphPad software). *P* values ≤0.05 indicated significant differences.

Supporting Information

Figure S1 Cholinergic neuronal marker-positive cells were observed in hiPS cell-derived neuronal cells. Expression levels of ChAT (A) and VAChT (B) were quantified by qPCR (n = 3) and normalized by that of GAPDH. "Fold expression" represents the ratio of expression on the given day compared to day 38. ChAT- (C) and VAChT (D)-positive cells were observed a little at day 52.
(TIF)

Figure S2 Percentages of the three isoforms of APP (APP770, APP751, and APP695) at 38, 45, and 52 days. Each column represents mean ± SD of 8 assays. $^{*}p<0.05$, $^{**}p<0.01$, $^{***}p<0.001$, Tukey's test.
(TIF)

Figure S3 New hsAPPα and sAPPβ antibodies specifically detect human sAPPα and sAPPβ by western blots, respectively. Human neuroglioma H4 cells overexpressing wild-type APP (APP_{WT}-H4 cells) were treated with α-secretase activator (12-*O*-tetradecanoylphorbol 13-acetate (TPA)), α-secretase inhibitor (TNF-α protease inhibitor-2 (TAPI-2)), or β-secretase inhibitor (see Protocol S1). Brain lysates of APP-knockout mice (APP-KO) were used as negative control. Immunoblots of conditioned media and supernatants of brain lysates were probed by anti-hsAPPα or anti-sAPPβ antibody. sAPPα or sAPPβ derived from both exogenous APP695 and endogenous APP770/751 are detected by each antibody. The increase in sAPPα by α-secretase activator and the reduction in sAPPα by α-secretase inhibitor effectively reached 434% and 50% of control (DMSO), respectively (upper panel). The decrease in sAPPβ by β-secretase inhibitor effectively reached 11% of control (lower panel). Neither sAPPα nor sAPPβ in the APP-KO brain was detected by anti-hsAPPα or anti-sAPPβ antibody, respectively. An asterisk indicates a non-specific band.
(TIF)

Figure S4 Immunocytochemical characterization of human ES cell (H9)-derived neuronal cells. (A) Time-dependent morphological changes of cells reseeded in a 24-well plate. Neuronal and glial cells were stained by anti-Tuj1 (left; red), anti-synapsin I (left; green), anti-MAP2 (right; red), and anti-GFAP (right; green) antibodies and DAPI (right; blue) at 38, 45, and 52 days. Scale bar, left; 20 μm, right; 50 μm. (B) ICC staining of Tbr1-, Ctip2-, Cux1- and Satb2-positive cells at day 52. (C–E) Neurotransmitter phenotypes at day 52. PAG (red)- and GAD (green)-positive (C), Glut1 (green)- and Tuj1 (red)-positive (D), and GABA (green)- and Tuj1 (red)-positive cells (E). Blue, DAPI. Scale bar, 50 μm.
(TIF)

Figure S5 Aβ production was modulated by several drugs in human ES cell-derived neuronal cells. β-Secretase inhibitor (BSI) (A, B), γ-secretase inhibitor (GSI) (C, D), and NSAID (E, F) were added into hES cell-derived neuronal cell cultures at day 36 (dotted line) and 50 (bold line), and two days later amounts of Aβ40 and Aβ42 secreted into the conditioned media were measured. The ratios Aβ40/FL-APP and Aβ42/FL-APP are expressed as percentages of the vehicle-treated group at day 52 and represent mean ± SD of 3 assays. *, $^{\#}p<0.05$, **, $^{\#\#}p<0.01$, ***, $^{\#\#\#}p<0.001$, significantly different from respective vehicle-treated groups by Dunnett's test.
(TIF)

Figure S6 Expression levels of reprogramming factors of iPS cells in neural differentiation. Total and transgene (Tg) expression levels of Sox2, Oct3/4 and Klf4 were measured by qPCR. Bold and dotted lines represent total and transgene expressions, respectively. "Fold expression" represents the ratio of the expression level compared to the total expression level at day 0 (iPS cells).
(TIF)

Figure S7 Aβ production was modulated by GSI in human iPS cell (201B7)-derived neuronal cells. γ-Secretase inhibitor (GSI) was added into the hiPS cell line, 201B7-derived neuronal cell cultures at day 36 (dotted line) and 50 (bold line), and two days later amounts of Aβ40 (A) and Aβ42 (B) secreted into the conditioned media were measured. The ratios Aβ40/FL-APP and Aβ42/FL-APP are expressed as percentages of the vehicle-treated group at day 52 and represent mean ± SD of 3 assays.
(TIF)

Protocol S1 Sampling method for checking antibody specificity.
(PDF)

Table S1 Effects of secretion inhibitors on cell viability measured by LDH assay at day 52.
(DOCX)

Table S2 qPCR primers.
(DOCX)

Acknowledgments

We would like to express our sincere gratitude to all our coworkers and collaborators, especially to K. Watanabe (RIKEN Brain Science Institute & Nagasaki University) for technical assistance and to K. Murai (CiRA) for editing manuscript.

Author Contributions

Conceived and designed the experiments: NI HI NY MA. Performed the experiments: NY MA NI. Analyzed the data: NY MA NI HI. Contributed reagents/materials/analysis tools: SK KT IA HH TK KM TCS TN TA SY. Wrote the paper: NY MA SY NI HI.

References

1. Selkoe DJ (2002) Alzheimer's disease is a synaptic failure. Science 298: 789–791.
2. Iwata N, Higuchi M, Saido TC (2005) Metabolism of amyloid-β peptide and Alzheimer's disease. Pharmacol Ther 108: 129–148.
3. Kukar TL, Ladd TB, Bann MA, Fraering PC, Narlawar R, et al. (2008) Substrate-targeting γ-secretase modulators. Nature 453: 925–929.
4. Kounnas MZ, Danks AM, Cheng S, Tyree C, Ackerman E, et al. (2010) Modulation of γ-secretase reduces β-amyloid deposition in a transgenic mouse model of Alzheimer's disease. Neuron 67: 769–780.
5. Takahashi K, Tanabe K, Ohnuki M, Narita M, Ichisaka T, et al. (2007) Induction of pluripotent stem cells from adult human fibroblasts by defined factors. Cell 131: 861–872.
6. Yu J, Vodyanik MA, Smuga-Otto K, Antosiewicz-Bourget J, Frane JL, et al. (2007) Induced pluripotent stem cell lines derived from human somatic cells. Science 318: 1917–1920.
7. Watanabe K, Kamiya D, Nishiyama A, Katayama T, Nozaki S, et al. (2005) Directed differentiation of telencephalic precursors from embryonic stem cells. Nat Neurosci 8: 288–296.
8. Gaspard N, Bouschet T, Hourez R, Dimidschstein J, Naeije G, et al. (2008) An intrinsic mechanism of corticogenesis from embryonic stem cells. Nature 455: 351–357.
9. Eiraku M, Watanabe K, Matsuo-Takasaki M, Kawada M, Yonemura S, et al. (2008) Self-organized formation of polarized cortical tissues from ESCs and its active manipulation by extrinsic signals. Cell Stem Cell 3: 519–532.
10. Li XJ, Zhang X, Johnson MA, Wang ZB, Lavaute T, et al. (2009) Coordination of sonic hedgehog and Wnt signaling determines ventral and dorsal telencephalic neuron types from human embryonic stem cells. Development 136: 4055–4063.
11. Zeng H, Guo M, Martins-Taylor K, Wang X, Zhang Z, et al. (2010) Specification of region-specific neurons including forebrain glutamatergic neurons from human induced pluripotent stem cells. PLoS One 5: e11853.
12. Chambers SM, Fasano CA, Papapetrou EP, Tomishima M, Sadelain M, et al. (2009) Highly efficient neural conversion of human ES and iPS cells by dual inhibition of SMAD signaling. Nat Biotechnol 27: 275–280.
13. Braak H, Braak E (1991) Neuropathological stageing of Alzheimer-related changes. Acta Neuropathol 82: 239–259.
14. Nakagawa M, Koyanagi M, Tanabe K, Takahashi K, Ichisaka T, et al. (2008) Generation of induced pluripotent stem cells without Myc from mouse and human fibroblasts. Nat Biotechnol 26: 101–106.
15. Wada T, Honda M, Minami I, Tooi N, Amagai Y, et al. (2009) Highly efficient differentiation and enrichment of spinal motor neurons derived from human and monkey embryonic stem cells. PLoS One 4: e6722.
16. Saito T, Hanai S, Takashima S, Nakagawa E, Okazaki S, et al. (2011) Neocortical layer formation of human developing brains and lissencephalies: consideration of layer-specific marker expression. Cereb Cortex 21: 588–596.
17. Kim JE, O'Sullivan ML, Sanchez CA, Hwang M, Israel MA, et al. (2011) Investigating synapse formation and function using human pluripotent stem cell-derived neurons. Proc Natl Acad Sci U S A 108: 3005–3010.
18. Akiyama H, Kaneko T, Mizuno N, McGeer PL (1990) Distribution of phosphate-activated glutaminase in the human cerebral cortex. J Comp Neurol 297: 239–252.
19. Blennow K, de Leon MJ, Zetterberg H (2006) Alzheimer's disease. Lancet 368: 387–403.
20. Kitazume S, Tachida Y, Kato M, Yamaguchi Y, Honda T, et al. (2010) Brain endothelial cells produce amyloid β from amyloid precursor protein 770 and preferentially secrete the O-glycosylated form. J Biol Chem 285: 40097–40103.
21. Yang LB, Lindholm K, Yan R, Citron M, Xia W, et al. (2003) Elevated β-secretase expression and enzymatic activity detected in sporadic Alzheimer disease. Nat Med 9: 3–4.
22. O'Connor T, Sadleir KR, Maus E, Velliquette RA, Zhao J, et al. (2008) Phosphorylation of the translation initiation factor eIF2α increases BACE1 levels and promotes amyloidogenesis. Neuron 60: 988–1009.
23. Parks AL, Curtis D (2007) Presenilin diversifies its portfolio. Trends Genet 23: 140–150.
24. Serneels L, Van Biervliet J, Craessaerts K, Dejaegere T, Horré K, et al. (2009) γ-Secretase heterogeneity in the Aph1 subunit: relevance for Alzheimer's disease. Science 324: 639–642.
25. McGowan E, Pickford F, Kim J, Onstead L, Eriksen J, et al. (2005) Aβ42 is essential for parenchymal and vascular amyloid deposition in mice. Neuron 47: 191–199.
26. Ono K, Condron MM, Ho L, Wang J, Zhao W, et al. (2008) Effects of grape seed-derived polyphenols on amyloid β-protein self-assembly and cytotoxicity. J Biol Chem 283: 32176–32187.
27. Hsiao K, Chapman P, Nilsen S, Eckman C, Harigaya Y, et al. (1996) Correlative memory deficits, Aβ elevation, and amyloid plaques in transgenic mice. Science 274: 99–102.
28. Kawarabayashi T, Younkin LH, Saido TC, Shoji M, Ashe KH, et al. (2001) Age-dependent changes in brain, CSF, and plasma amyloid β protein in the Tg2576 transgenic mouse model of Alzheimer's disease. J Neurosci 21: 372–381.
29. Mehta PD, Pirttilä T, Mehta SP, Sersen EA, Aisen PS, et al. (2000) Plasma and cerebrospinal fluid levels of amyloid β proteins 1-40 and 1-42 in Alzheimer disease. Arch Neurol 57: 100–105.
30. Asai M, Iwata N, Tomita T, Iwatsubo T, Ishiura S, et al. (2010) Efficient four-drug cocktail therapy targeting amyloid-β peptide for Alzheimer's disease. J Neurosci Res 88: 3588–3597.
31. Stachel SJ, Coburn CA, Steele TG, Jones KG, Loutzenhiser EF, et al. (2004) Structure-based design of potent and selective cell-permeable inhibitors of human β-secretase (BACE-1). J Med Chem 47: 6447–6450.
32. Seiffert D, Bradley JD, Rominger CM, Rominger DH, Yang F, et al. (2000) Presenilin-1 and -2 are molecular targets for γ-secretase inhibitors. J Biol Chem 275: 34086–34091.
33. Weggen S, Eriksen JL, Das P, Sagi SA, Wang R, et al. (2001) A subset of NSAIDs lower amyloidogenic Aβ42 independently of cyclooxygenase activity. Nature 414: 212–216.
34. Eriksen JL, Sagi SA, Smith TE, Weggen S, Das P, et al. (2003) NSAIDs and enantiomers of flurbiprofen target γ-secretase and lower Aβ 42 in vivo. J Clin Invest 112: 440–449.
35. Burton CR, Meredith JE, Barten DM, Goldstein ME, Krause CM, et al. (2008) The amyloid-β rise and γ-secretase inhibitor potency depend on the level of substrate expression. J Biol Chem 283: 22992–23003.
36. Games D, Adams D, Alessandrini R, Barbour R, Berthelette P, et al. (1995) Alzheimer-type neuropathology in transgenic mice overexpressing V717F β-amyloid precursor protein. Nature 373: 523–527.
37. De Meyer G, Shapiro F, Vanderstichele H, Vanmechelen E, Engelborghs S, et al. (2010) Diagnosis-independent Alzheimer disease biomarker signature in cognitively normal elderly people. Arch Neurol 67: 949–956.
38. Inoue H, Yamanaka S (2011) The use of induced pluripotent stem cells in drug development. Clin Pharmacol Ther 89: 655–661.
39. Iwatsubo T, Saido TC, Mann DM, Lee VM, Trojanowski JQ (1996) Full-length amyloid-β (1-42(43)) and amino-terminally modified and truncated amyloid-β 42(43) deposit in diffuse plaques. Am J Pathol 149: 1823–1830.
40. Johnson MA, Weick JP, Pearce RA, Zhang SC (2007) Functional neural development from human embryonic stem cells: accelerated synaptic activity via astrocyte coculture. J Neurosci 27: 3069–3077.
41. Lazarov O, Lee M, Peterson DA, Sisodia SS (2002) Evidence that synaptically released β-amyloid accumulates as extracellular deposits in the hippocampus of transgenic mice. J Neurosci 22: 9785–9793.
42. Soba P, Eggert S, Wagner K, Zentgraf H, Siehl K, et al. (2005) Homo- and heterodimerization of APP family members promotes intercellular adhesion. EMBO J 24: 3624–3634.
43. Woo SM, Kim J, Han HW, Chae JI, Son MY, et al. (2009) Notch signaling is required for maintaining stem-cell features of neuroprogenitor cells derived from human embryonic stem cells. BMC Neurosci 10: 97.
44. Mangialasche F, Solomon A, Winblad B, Mecocci P, Kivipelto M (2010) Alzheimer's disease: clinical trials and drug development. Lancet Neurol 9: 702–716.
45. Qiang L, Fujita R, Yamashita T, Angulo S, Rhinn H, et al. (2011) Directed conversion of Alzheimer's disease patient skin fibroblasts into functional neurons. Cell 146: 359–371.
46. Kaneko T, Urade Y, Watanabe Y, Mizuno N (1987) Production, characterization, and immunohistochemical application of monoclonal antibodies to glutaminase purified from rat brain. J Neurosci 7: 302–309.
47. Saido TC, Nagao S, Shiramine M, Tsukaguchi M, Sorimachi H, et al. (1992) Autolytic transition of mu-calpain upon activation as resolved by antibodies distinguishing between the pre- and post-autolysis forms. J Biochem 111: 81–86.

RESEARCH ARTICLE

International Journal of Geriatric Psychiatry

Relationship between white matter T2 hyperintensity and cortical volume changes on magnetic resonance imaging in healthy elders

Miho Ota[1,2], Kiyotaka Nemoto[2], Noriko Sato[1], Katsutoshi Mizukami[3], Fumio Yamashita[4] and Takashi Asada[3]

[1]Department of Radiology, National Center of Neurology and Psychiatry, Ogawahigashi, Kodaira, Tokyo, Japan
[2]Division of Psychiatry, Tsukuba University Hospital, Amakubo, Tsukuba, Ibaraki, Japan
[3]Departments of Neuropsychiatry, Institute of Clinical Medicine, University of Tsukuba, Tennoudai, Tsukuba, Ibaraki, Japan
[4]Department of Psychiatry, Institute of Clinical Medicine, University of Tsukuba, Tennoudai, Tsukuba, Ibaraki, Japan
Correspondence to: M. Ota, E-mail: ota@ncnp.go.jp

Objective: T2 white matter hyperintensity (WMH) on magnetic resonance imaging (MRI) is associated with brain atrophy. Some previous studies examined the relation between the WMH and cortical atrophy, however, little is known about how the WMHs affect the pattern of cortical atrophy. Recent studies have revealed that patho-physiological role of WMH in affecting cortical atrophy may be different between hyperintensities in basal ganglia and thalami (B&T) and those in other regions. Based on a longitudinal study up to 5 years, we attempt to examine the temporal relation between the WMHs and cortical atrophy with special attention to the hyperintensities in the B&T.

Methods: We evaluated the temporal pattern of cortical atrophy in 74 cognitively normal subjects lacking hyperintensities in B&T (first analysis) and 13 cognitively normal subjects with hyperintensities in B&T (second analysis). The relationship between the baseline WMH severity and the cortical volume change during the observation period (mean: 3.8 years) was voxel basically evaluated on the images.

Results: The first analysis showed fairly axisymmetrical atrophy pattern in parietal, occipital, and precentral cortices, while the findings gained from the second appear to lack such systematic orderliness of the atrophy.

Conclusion: This result shows that WMH may affect atrophy in multiple cerebral cortices even in cognitively normal subjects. Understanding the impact of WMH on the shrinkage shown in the brains of cognitively healthy older individuals is an important base for assessing the temporal pattern of atrophy of the individual with neurodegenerative disorder like AD. Copyright © 2010 John Wiley & Sons, Ltd.

Key words: white matter hyperintensity; magnetic resonance imaging; older
History: Received 15 June 2010; Accepted 21 July 2010; Published online 24 September 2010 in Wiley Online Library (wileyonlinelibrary.com).
DOI: 10.1002/gps.2618

Introduction

White matter hyper-intensities (WMH) defined as areas with high signal intensities on T2-weighted magnetic resonance imaging (MRI) are commonly found on MRI of older individuals. They have been reported to be related with cognitive impairment and vascular pathology even in the healthy older. The WMH affect cognitive function including the speed of cognitive processes and executive function (Junqué *et al.*, 1990; Schmidt *et al.*, 1993), which is presumably associated with brain atrophy and reduced cerebral blood flow (Mirsen *et al.*, 1991; De Reuck *et al.*, 1992; Du *et al.*, 2005; Mungas *et al.*, 2005; Wen *et al.*, 2006). Pathology of WMH may be attributable to dilatation of periventricular space, peri-vascular demyelination, and gliosis. Several researchers have examined the patho-physiological role of WMH in affecting cortical atrophy of the healthy and pathological brains of the older.

Recently, mild cognitive impairment (MCI) which is a distinct state of abnormal cognition that does not amount to dementia but is distinguishable from

normal cognitive decline associated with aging has attracted an increasing attention, because it may offer opportunities for very early diagnosis of Alzheimer's disease (AD). One study reported that high WMH prevalence strongly predicted the progression from normal to MCI (Smith *et al.*, 2008).

Another study showed difference in the level of WMH between the MCI to AD converter and non-converters (Misra *et al.*, 2009). Although whether the patho-physiology of AD is directly associated with vascular pathological changes remain an open question, it appears that the clinical manifestation of AD is highly correlated with the vascular pathology (Misra *et al.*, 2009). AD patients are likely to have more extensive WMH than age-matched controls (Scheltens *et al.*, 1992).

Taking such information into consideration, it is very important to examine the pattern and mechanism of WMH on cortical atrophy among cognitively healthy individuals is very important for the basis of the assessment for the pattern and mechanism among individuals with pathological conditions including AD.

Most of the previous studies regarding the association between WMH and the cortical atrophy examined the correlation between the load for whole brain WMHs and shrinkage of whole brain gray matter (Mirsen *et al.*, 1991; Du *et al.*, 2005; Mungas *et al.*, 2005), thus little is known about the effect of WMH on the regional cortical atrophy. An exceptional study reported that the WMHs in the frontal lobe were correlated with the change in the volume of frontal cortex (Tullberg *et al.*, 2004). Another study also showed that subjects with WHM loads located mainly in frontal lobe showed bilateral frontal cortical atrophy (Rossi *et al.*, 2006). Furthermore, a study showed the correlation between the cortical change of each lobe and WMHs in its corresponding white matter (Wen *et al.*, 2006). It is of note that all of these studies are cross-sectional design, and no previous study has examined the relation longitudinally.

Recent development of the diffusion tensor imaging technique enabled the depiction of projecting neural fibers non-invasively (Behrens *et al.*, 2003). The development has revealed that basal ganglia and thalami (B&T) mediate communication over widespread areas of the cortex with neural fibers as the central relay station in the brain. The hyperintensity in T2-weighted images of B&T may affect not only volume change of themselves but also the cerebral cortex to which B&T connect. In addition, some researchers have reported that the disturbance of cerebral cortex conversely affects the volume change of basal ganglia (Ogawa *et al.*, 1997; Ota *et al.*, 2007). Therefore, for the accurate estimation of the influence of the WMH on cortical volume loss, it may be appropriate that hyperintensity on T2-weighted images in B&T and that in other regions should be dealt separately. However, previous quantitative studies, automatically calculated the volume of WMHs of the whole brain, thus they did not distinguish hyperintensities on T2-weighted image in B&T from those in other regions. Some studies evaluated the relationship between the regional cortical volume and the WMH loads voxel based on a lobe-to-lobe basis (Rossi *et al.*, 2006; Wen *et al.*, 2006). However, it is known that WMHs in any brain region cause other cortical changes (Tullberg *et al.*, 2004; Rossi *et al.*, 2006; Wen *et al.*, 2006). Additionally, because too many factors are involved in the interaction, it is difficult to evaluate the relationship between the atrophy and the WMHs.

In this study, we have conducted a follow-up brain MRI study for the older individuals participating in a community-based study. In order to easily exclude the subjects with hyperintensities in B&T, we adopted qualitative morphometry based on the grading of local WMHs and identified the subjects without hyperintensities on T2-weighted image in B&T. We examined the correlation between the severity of baseline-scan WMH for whole brain and the atrophy rate of the regional cortex using voxel-based morphometry.

Methods

This study was conducted as a part of a community-based project aiming at prevention of dementia in the older. The details of the project have been reported elsewhere, so the description of the method here will be given in brief (Miyamoto *et al.*, 2009). The protocol for this study was approved by the ethics committee of the University of Tsukuba and all participants gave their informed consent.

At the baseline, between December 2001 and April 2002, 1888 out of the 2698 candidate inhabitants who were 65 years or older underwent the cognitive assessment using a battery of neuropsychological tests (Sasaki *et al.*, 2009); category-cued recall (Grober *et al.*, 1998); set-dependency activity (Sohlberg and Mateer, 1986); category verbal fluency (Monsch *et al.*, 1992); clock-drawing test (Brodaty and Moore, 1997); and Wechsler Adult Intelligence Scale Revised (WAIS-R) (Wechsler, 1981). We regarded the subject who marked score less than 1 SD below the demographically corrected mean on each of the five cognitive domains to fall short of normal limits (Miyamoto *et al.*, 2009).

According to our invitation, 284 self-selected subjects underwent brain MRI scanning. A total of 172 individuals out of the 284 were diagnosed as having normal cognitive function and no abnormal MRI findings such as cortical infarctions, brain tumors, or head injury. We defined infarct as high intensity lesion having a size of ≧3 mm on T2-weighted images and low intensity on T1-weighted images, following the criteria of the Workshop Study (Adachi *et al.*, 2002). They were selected as the participants for the present longitudinal MRI study. Using Fazekas criterion for the severity of WMH, we defined Fazekas 2 or 3 as severe hyperintensity (Wahlund *et al.*, 2001).

Eighty-seven out of the 172 participants were cognitively healthy both at the baseline and the end of the observation period, and underwent annual MRI scanning at least four times. From these 87 participants, we excluded 13 subjects with severe hyperintensity located in B&T on the images of the baseline-scan. For the first analysis, the data from cognitively healthy 74 subjects (39 men, 35 women; mean age, 72.3 ± 3.8 years; mean years of education, 10.9 ± 3.1 years; mean mini-mental state examination (MMSE) score, 28.4 ± 1.8 at the baseline, scan interval = 3.8 ± 0.2) lacking hyperintensities in B&T were used. For the second analysis, the 13 subjects with severe hyperintensities in B&T (4 men, 9 women; mean age, 75.4 ± 4.4 years; mean years of education, 10.4 ± 3.2 years; mean MMSE score, 27.8 ± 2.4 at the baseline, scan interval = 3.8 ± 0.1) were employed.

The clinical characteristics of the subjects are presented in Table 1. We used a pair of MRI data with for each participant.

First, cranial MRI was performed using a 1.5-T Magnetom Symphony system (Siemens, Erlangen, Germany). Conventional axial T2-weighted turbo spin echo images were obtained using the following settings: repetition time (TR), 4000 ms; echo time (TE), 96 ms; slice thickness, 5 mm; intersection gap, 1.5 mm; matrix, 512 × 512; field of view, 230 × 230 mm; number of signals acquired, 2. In addition to T2-weighted imaging, high spatial-resolution, 3-dimensional (3D) T1-weighted imaging was also used for the study. Scans for 3D T1-weighted imaging were made in the sagittal plane using the following settings: TR, 2080 ms; TE, 3.93 ms; flip angle, 12°; effective section thickness, 1.20 mm; slab thickness, 173 mm; matrix, 512 × 512; field of view, 280 × 280 mm; number of signals acquired, 1. This yielded 144 contiguous slices through the head.

To clarify the relationship between the rate of cortical gray matter volume change and the severity of WMH, structural 3D T1-weighted MR images were analyzed using an optimized voxel-based morphometry (VBM) technique. Data were computed using Statistical Parametric Mapping 5 (SPM5) software (Wellcome Department of Imaging Neuroscience, London, UK) running on MATLAB 7.0 (Math Works, Natick, MA). Optimized VBM were processed using SPM5 tool software. Details of this process are described elsewhere (Good *et al.*, 2001). Normalized segmented images were modulated by multiplication with Jacobian determinants of spatial normalization function to encode the deformation field for each subject as tissue density changes in normal space. The atrophy rate of the regional gray matter was computed by comparing the modulated segmented scan image

Table 1 Descriptive characteristics of the study sample without white matter hyperintensities in basal ganglia and thalami (Fazekas <2; (a), $N = 74$) and with hyperintensities in basal ganglia and thalami (Fazekas ≧2; (b), $N = 13$)

The degree of subcortical white matter changes	Age (year) (quartile; median)	Sex	MRI period (year) (quartile; median)	Education (year) (quartile; median)	MMSE (quartile; median)
(a)					
Fazekas = 0	69–73 71	M: 23; F: 24	3.6–3.8 3.7	8–12 11	27–30 29
Fazekas = 1	69.8–74.5 72	M: 11; F: 5	3.7–3.8 3.7	11–12 12	27–30 29
Fazekas = 2	75–78 77	M: 4; F: 5	3.7–3.8 3.7	8–12 8	28–30 30
Fazekas = 3	76–78 (range)	M: 1; F: 1	3.6–3.8 (range)	11–11 (range)	27–30 (range)
(b)					
Fazekas = 0		M: 0; F: 0			
Fazekas = 1	72.5–75.8 74	M: 1; F: 3	3.8–4.0 3.9	8.3–11.5 9.5	28.8–30 29.5
Fazekas = 2	73.5–78 76	M: 2; F: 5	3.7–3.8 3.8	8–17 12.5	25–29.5 26
Fazekas = 3	74–76 (range)	M: 1; F: 1	3.8–3.9 (range)	8–17 (range)	25–30 (range)

at the baseline (I_b) and at the follow up (I_f) (Fotenos *et al.*, 2005).

$$\text{Atrophy rate} = \frac{(I_b - I_f)}{I_b}$$

Images of the atrophy rate were smoothed using a 8 mm full-width half-maximum of an isotropic Gaussian kernel.

For the present analysis, we took the severity of WMH into consideration. The levels for overall severity of white matter excluding B&T were divided into four: 0, no lesion; 1, focal lesions in at least one lobe; 2, beginning confluence of lesions in at least one lobe; 3, diffuse lesions in all over white mattes (Figure 1), and 0, no lesion; 1, focal lesions; 2, >1 focal lesions, and 3, confluent lesions for B&T (DeCarli *et al.*, 2005).

Two trained operators rated the overall severity for white matter excluding B&T and the severity of B&T of the 84 participants, and the reproducibility was calculated. The intra-class correlation coefficients (ICCs) for these measurements were 0.85 and 0.95, respectively. ICC values over 0.75 indicate good reliability, so our rating is considered to be reliable (Landis and Koch, 1977).

The relationship between the atrophy rate of regional gray matter volume and the severity of WMH at the baseline scan was evaluated using a single regression model. Only correlations that had a cluster level of $p < 0.001$ (uncorrected) with an extent threshold criterion of more than 300 contiguous voxels were considered statistically to be significant. For the evaluation of the effect of WMH on the gray matter volume, the result was masked with the gray matter image derived from the WFU_pickatlas (Maldjian *et al.*, 2003). Subsequently, we evaluated the correlation between severity of the WMH and progression of the brain atrophy using age as a nuisance variable. We regarded the criteria same as above (a cluster level of $p < 0.001$ (uncorrected) with an extent threshold criterion of more than 300 contiguous voxels) as statistically significant, too. Only this process, statistical analysis was performed using SPM2.

We also evaluated the differences among the four levels (Fazekas = 0, 1, 2, and 3) according to age, sex, MMSE score, years of education, and scan interval using one-way ANOVA. Statistical analyses were performed using SPSS for Windows 11.0.1J software (SPSS Japan, Tokyo, Japan).

Results

The first analysis for the 74 subjects lacking hyperintensities in B&T showed significant positive correlations between the atrophy rate of regional gray matter and severity of WMH in the bilateral parietal and occipital cortices axisymmetrically, birateral precentral gyri, and right frontal cortex (Figure 2). The analyses showed no significant difference in sex, MMSE score, years of education, and scan interval among the four groups. However, only a significant difference in age

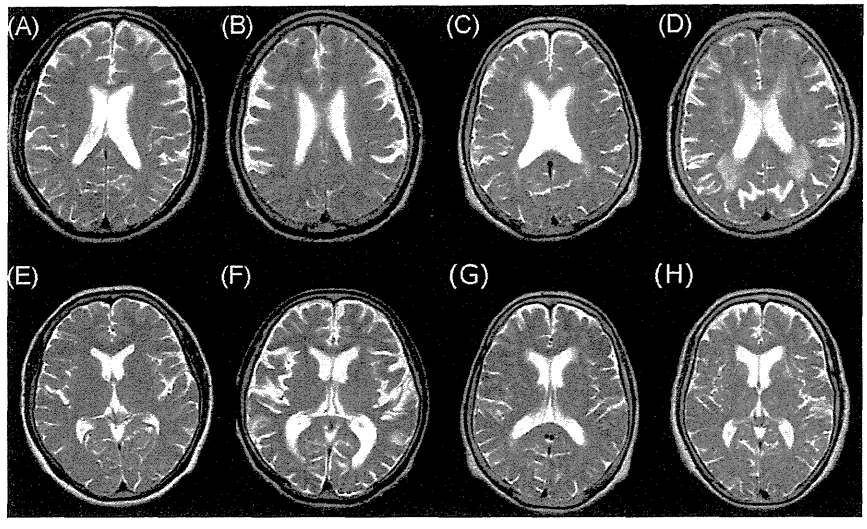

Figure 1 (A–H) Examples of rating scores 0, 1, 2, and 3 on cerebral T2-weighted imaging. Upper column: definitions of rating scores for white matter lesions: 0, no lesion (A); 1, focal lesions (B); 2, beginning confluence of lesions (C); 3, diffuse lesions in all over white mattes (D). Lower column: definitions of rating scores for basal ganglia and thalami: 0, no lesion (E); 1, focal lesions (F); 2, >1 focal lesions (G), and 3, confluent lesions (H).

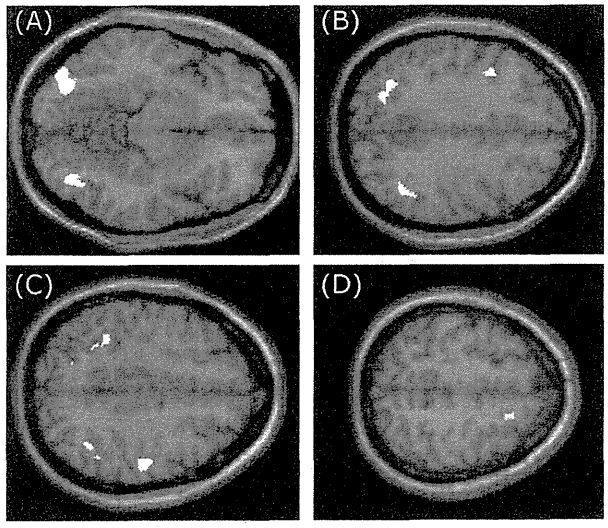

Figure 2 The relationship between the atrophy rate of regional gray matter volume and WMH severity at the baseline scan was evaluated in 74 participants without the hyperintensity in basal ganglia (single regression model, SPM5). There were positive correlations between WMH severity and the atrophy rate of the regional gray matter volume of (A) the bilateral occipital corti, (B) the bilateral parietal corti and left precentral gyrus, (C) the right precentral gyrus, and (D) right frontal cortex.

was observed between groups with Fazekas = 0 and Fazekas = 2 groups. Further, the subsequent analysis evaluating the correlation between severity of the WMH and atrophy rate using age as a nuisance variable showed significant positive correlations between the atrophy rate of regional gray matter and severity of WMH in the bilateral parietal and occipital cortices nearly axisymmetrically (Figure 3).

The second analysis using the data from 13 participants with hyperintensities in B&T showed only a slightly positive correlation between severity of WMHs and the atrophy rate of regional gray matter in the left parietal gyrus at the trend level (Figure 4; a seed level of $p < 0.01$ (uncorrected)).

In sum, the first analysis showed fairly axisymmetrical pattern, while the findings gained from the second analysis appear to lack systematic orderliness.

Discussion

The first analysis showed significantly positive correlations between the atrophy rate of gray matter and the severity of WMH at the baseline scan in the bilateral frontal, occipital and parietal lobes almost axisymmetrically (Figure 2). However, the second did not replicate the findings.

Previous studies showed that WMHs in any brain region cause other cortical changes (Tullberg *et al.*, 2004; Rossi *et al.*, 2006; Wen *et al.*, 2006). In addition, a study showed that there were correlations not only between WMH volume in each subdivided region and WMH volume for the overall brain, but also among each WMH volume in subdivided regions, respectively (DeCarli *et al.*, 2005). On the other hand, there are too many factors involved in the interaction to evaluate the relationship between the atrophy and the WMHs. Therefore, for the simplicity purpose, we regarded the severity of WMH for overall brain as the individual index for the subcortical WMH severity.

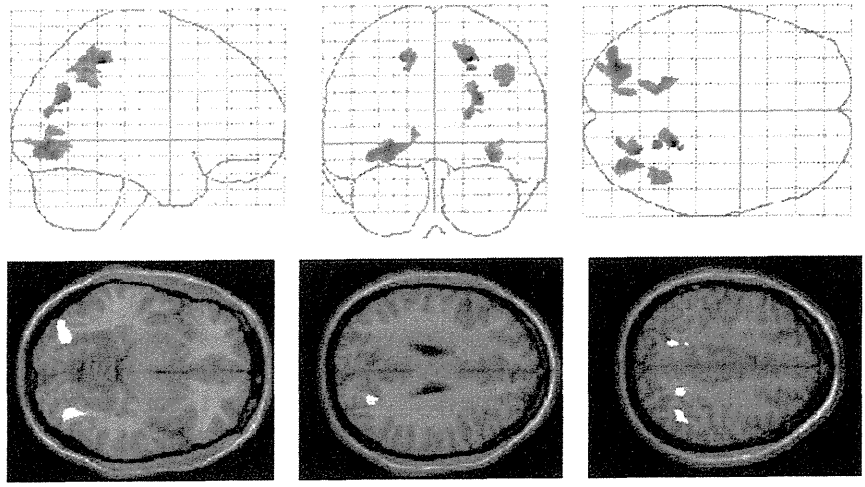

Figure 3 The relationship between the atrophy rate of regional gray matter volume and WMH severity at the baseline scan using the age as nuisance variable was evaluated in 74 participants without the hyperintensity in basal ganglia (SPM2). There were positive correlations between WMH severity and the atrophy rate of the regional gray matter volume of the bilateral occipital and parietal corti.

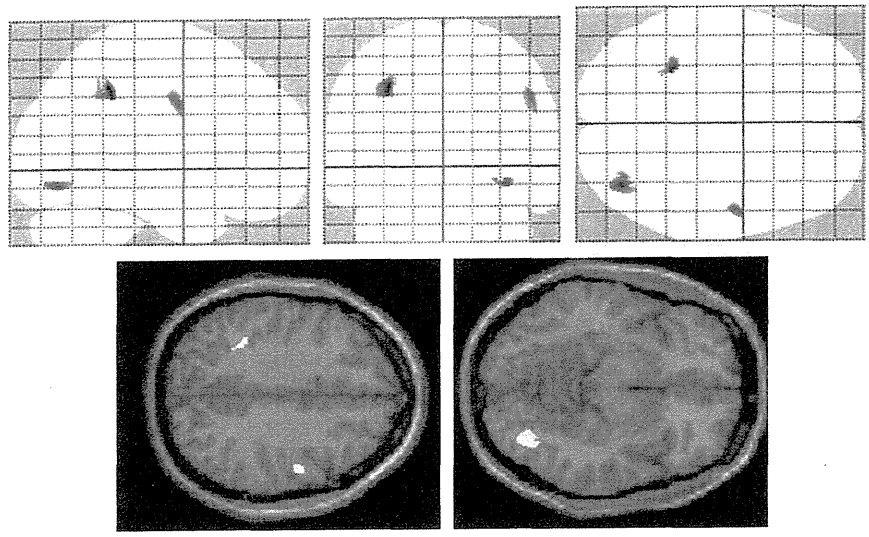

Figure 4 There was a positive correlation between severity of hyperintensity and the atrophy rate of regional gray matter volume of the left parietal cortex at the trend level in 13 participants with the severe hyperintensity in basal ganglia and thalamus.

Our results showing the relationship between the severity of WMH and the atrophy rate is compatible with previous result in general. It is known that WMH loads are likely to be observed in the white matter around the frontal horn of the lateral cerebral ventricle in the frontal lobes, and the posterior horn of the lateral cerebral ventricle in the parieto-occipital lobes, and WMH were distributed symmetrically (Wahlund *et al.*, 2001; Yoshita *et al.*, 2006). Others showed that frontal and parieto-occipital regions are the most common sites for WMH (Tullberg *et al.*, 2004; Rossi *et al.*, 2006). Our study duplicated such distribution pattern of WMH. Our result of the cerebral shrinkage and the severity of whole brain WMH might be mainly explained by the correlation between the shrinkage of the cortex in the frontal, parietal, and occipital lobes and the severity of WMH in their respective lobes. Further, the additional analysis evaluating the relationship between the severity of the WMH and atrophy rate without the aging effect showed significant positive correlations between the atrophy rate of gray matter and the severity of WMH in the bilateral occipital and parietal lobes axisymmetrically, but not in frontal regions. These fingins showed in occipito-parietal regions were nearly the same as the results not excluding the aging effect. Aging disproportionately affects frontal lobe structure, and leaving posterior and inferior brain regions relatively intact (Pfefferbaum *et al.*, 2005). In this regard, the confounding factor, aging effect, may affect these viewpoints.

Hyperintensities in the B&T mediating vast communication over widespread areas of the cortex (Mungas *et al.*, 2005; Leh *et al.*, 2007) might induce volume change in not only the brain structures *per se*, but also the connected cerebral cortices. However, previous studies paid little attention to the hyperintensities in B&T, and these results not always indicate axisymmetrical correlation. In this point, our study is the first one that investigated the WMH and cortical volume with attention to the presence or absence of the hyperintensities in B&T. When considering B&T mediate vast communication over widespread cortex (Behrens *et al.*, 2003; Mungas *et al.*, 2005), hyperintensities in B&T might induce volume change in not only the brain structures *per se*, but also the connected cerebral cortices. The second analysis using the data from 13 subjects with hyperintensities in B&T showed the asymmetrical relationship between the atrophy rate and the WMH severity. Thus, the differences in the results may be attributable to the influence of the hyperintensities in B&T.

There is a limitation in this study. First, T2 images were acquired with slice thickness of 5 mm and gap of 1.5 mm. Although our participants showed no large ischemic lesion in B&T, it might be possible that WMH from small brain structures such as thalamus and basal ganglia may not be observed. Further work using thin slice thickness and gapless T2 image will be necessary to confirm our results. Second, we did not have a large enough number of subjects with WMH loads in the basal ganglia and thalami. The procedure to extract cognitively healthy subjects through several tests might have excluded or limited the subjects with WMH lesions, which affect cognitive ability. Further studies using a large group of subjects need to be conducted. Third, previous study showed the different efficacy

Key points

- We showed fairly axisymmetrical atrophy pattern in subjects without the hyperintensities in basal ganglia and thalami.
- The atrophy pattern of the cerebrum with the subjects with the hyperintensities in basal ganglia and thalami appear to lack systematic orderliness.
- This result shows that WMH may affect atrophy in multiple cerebral cortices even in cognitively normal subjects.

of the deep white matter hyperintensity and periventricular white matter hyperintensity on the brain atrophy (Wen *et al.*, 2006), and a fluid-attenuated inversion recovery (FLAIR) sequence may be more useful for assessment of WMH (DeCarli *et al.*, 2005). However, Fazekas = 3 group sometimes showed the contiguous white matter lesion from periventricular space to the deep white matter, and the number of Fazekas = 3 group were relatively small. So, we could not divide these findings. Further works concerning this point using the same method will be necessary. In addition, we evaluated the severity of WMH by qualitative method, not by quantitative one, and the previous study showed that the periventricular WMH and deep white matter hyperintensities were highly correlated with total WMH and with each other (DeCarli *et al.*, 2005). Consequently, we managed to show the statistically significant correlations. Further studies using a FLAIR sequence need to be conducted.

In conclusion, WMH are associated with shrinkage of every lobe even in cognitively normal subjects. Understanding the impact of WMH on the shrinkage shown in the brains of cognitively healthy older individuals is an important base for assessing the temporal pattern of atrophy of the individual with neurodegenerative disorder including AD.

Conflicts of interest

None declared.

References

Adachi T, Kobayashi S, Yamaguchi S. 2002. Frequency and pathogenesis of silent subcortical brin infactiono ain acute first-ever ischemic stroke. *Intern Medicine* **41**: 103–108.

Behrens TE, Johansen-Berg H, Woolrich MW, *et al.* 2003. Non-invasive mapping of connections between human thalamus and cortex using diffusion imaging. *Nat Neurosci* **6**: 750–757. [Pubmed: 12808459].

Brodaty H, Moore CM. 1997. The Clock Drawing Test for dementia of the Alzheimer's type: a comparison of three scoring methods in a memory disorders clinic. *Int J Geriatr Psychiatry* **12**: 619–627. [Pubmed: 9215942].

DeCarli C, Fletcher E, Ramey V, *et al.* 2005. Anatomical mapping of white matter hyperintensities (WMH): exploring the relationships between periventricular WMH, deep WMH, and total WMH burden. *Stroke* **36**: 50–55. [Pubmed: 15576652].

De Reuck J, Decoo D, Strijckmans K, *et al.* 1992. Does the severity of leukoaraiosis contribute to senile dementia? A comparative computerized and positron emission tomographic study. *Eur Neurol* **32**: 199–205. [Pubmed; 1505589].

Du AT, Schuff N, Chao LL, *et al.* 2005. White matter lesions are associated with cortical atrophy more than entorhinal and hippocampal atrophy. *Neurobiol Aging* **26**: 553–559. [Pubmed: 15653183].

Fotenos AF, Snyder AZ, Girton LE, *et al.* 2005. Normative estimates of cross-sectional and longitudinal brain volume decline in aging and AD. *Neurology* **64**: 1032–1039. [Pubmed: 15781822].

Good CD, Johnsrude I, Ashburner J, *et al.* 2001. Cerebral asymmetry and the effect of sex and handedness on brain structure: a voxel-based morphometric analysis of 465 normal adult human brains. *Neuroimage* **4**: 685–700. [Pubmed: 11506541].

Grober E, Buschke H, Crystal H, *et al.* 1998. Screening for dementia by memory testing. *Neurology* **38**: 900–903. [Pubmed: 3368071].

Junqué C, Pujol J, Vendrell P, *et al.* 1990. Leukoaraiosis on magnetic resonance imaging and speed of mental processing. *Arch Neurol* **47**: 151–156. [Pubmed: 2302086].

Landis JR, Koch GG. 1977. The measurement of observer agreement for categorical data. *Biometrics* **33**: 159–174. [Pubmed: 843571].

Leh SE, Ptito A, Chakravarty MM, *et al.* 2007. Fronto-striatal connections in the human brain: a probabilistic diffusion tractography study. *Neurosci Lett* **419**: 113–118. [Pubmed: 17485168].

Maldjian JA, Laurienti PJ, Burdette JB, *et al.* 2003. An automated method for neuroanatomic and cytoarchitectonic atlas-based interrogation of fMRI data sets. *NeuroImage* **19**: 1233–1239. [Pubmed: 12880848].

Mirsen TR, Lee DH, Wong CJ, *et al.* 1991. Clinical correlates of white-matter changes on magnetic resonance imaging scans of the brain. *Arch Neurol* **48**: 1015–1021. [Pubmed: 1929891].

Misra C, Fan Y, Davatzikos C. 2009. Baseline and longitudinal patterns of brain atrophy in MCI patients, and their use in prediction of short-term conversion to AD: results from ADNI. *Neuroimage* **44**: 1415–1422. [Pubmed: 19027862].

Miyamoto M, Kodama C, Kinoshita T, *et al.* 2009. The issue of non-responders: comparison of the prevalence of dementia and mild cognitive impairment among quick-, delayed-responders, and final-nonresponders to a community survey. *J Clin Neurosci* **16**: 270–276. [Pubmed: 19091575].

Monsch AU, Bondi MW, Butters N, *et al.* 1992. Comparisons of verbal fluency tasks in the detection of dementia of the Alzheimer type. *Arch Neurol* **49**: 1253–1258. [Pubmed: 1449404].

Mungas D, Harvey D, Reed BR, *et al.* 2005. Longitudinal volumetric MRI change and rate of cognitive decline. *Neurology* **65**: 561–571. [Pubmed: 16116117].

Ogawa T, Yoshida Y, Okudera T, *et al.* 1997. Secondary thalamic degeneration after cerebral infarction in the middle cerebral artery distribution: evaluation with MR imaging. *Radiology* **204**: 255–262. [Pubmed: 9205256].

Ota M, Obata T, Akine Y, *et al.* 2007. Laterality and aging of thalamic subregions measured by diffusion tensor imaging. *Neuroreport* **18**: 1071–1075. [Pubmed: 17558299].

Pfefferbaum A, Adalsteinsson E, Sullivan EV. 2005. Frontal circuitry degradation marks healthy adult aging: evidence from diffusion tensor imaging. *Neuroimage* **26**: 891–899. [Pubmed: 15955499].

Rossi R, Boccardi M, Sabattoli F, *et al.* 2006. Topographic correspondence between white matter hyperintensities and brain atrophy. *J Neurol* **253**: 919–927. [Pubmed: 16502217].

Sasaki M, Kodama C, Hidaka S, *et al.* 2009. Prevalence of four subtypes of mild cognitive impairment and APOE in a Japanese community. *Internat J Geriat Psychiat* **24**: 1119–1126. [Pubmed: 19449451].

Scheltens P, Barkhof F, Valk J, *et al.* 1992. White matter lesions on magnetic resonance imaging in clinically diagnosed Alzheimer's disease. Evidence for heterogeneity. *Brain* **115**: 735–748. [Pubmed: 1628199].

Schmidt T, Fazekas F, Offenbacher H, *et al.* 1993. Neuropsychologic correlates of MRI white matter hyperintensities: a study of 150 normal volunteers. *Neurology* **43**: 2490–2494. [Pubmed: 8255445].

Smith EE, Egorova S, Blacker D, *et al.* 2008. Magnetic resonance imaging white matter hyperintensities and brain volume in the prediction of mild cognitive impairment and dementia. *Arch Neurol* **65**: 94–100. [Pubmed: 18195145].

Sohlberg MM, Mateer CA. 1986. *Attention Process Training (APT)*. Association for Neuropsychological Research and Development: Puyallup, WA.

Tullberg M, Fletcher E, DeCarli C, *et al.* 2004. White matter lesions impair frontal lobe function regardless of their location. *Neurology* **63**: 246–253. [Pubmed; 15277616].

Wahlund LO, Barkhof F, Fazekas F, *et al.* 2001. European Task Force on age-related white matter changes. A new rating scale for age-related white matter changes applicable to MRI and CT. *Stroke* **32**: 1318–1322. [Pubmed: 11387493].

Wechsler D. 1981. *WAIS-R Manual*. The Psychological Corporation: New York.

Wen W, Sachdev P, Chen X, *et al.* 2006. Gray matter reduction is correlated with white matter hyperintensity volume: a voxel-based morphometric study in a large epidemiological sample. *Neuroimage* **29**: 1031–1039. [Pubmed: 16253521].

Yoshita M, Fletcher E, Harvey D, *et al.* Extent and distribution of white matter hyperintensities in normal aging, MCI, and AD. *Neurology* 2006. **67**: 2192–2198. [Pubmed: 17190943].

特集 認知症の生活機能障害

いわゆる巣症状の脳内メカニズム

Brain mechanisms of 'focal' neuropsychological signs in dementia

札幌医科大学医学部リハビリテーション医学講座教授
Sumio Ishiai 石合純夫

Summary

認知症では，失語，失行，失認，半側空間無視のような「いわゆる巣症状」が，脳卒中のように典型的に認められることはあまり多くない。しかし，言語，行為，物体・顔の認知，空間性注意の障害や遂行機能障害が起こることは紛れもない事実であり，認知症の診断において重視されている。一方，前向性健忘を中心とした記憶障害は，脳血管障害などによる限局性病巣がPapezの回路を損傷することによって起こることもあるが，アルツハイマー病の主症状として高頻度にみられる。これらの高次脳機能障害ないしは神経心理学的症状について，その発現に関わる脳内メカニズムを最近の神経ネットワークの考え方に重点を置いて解説する。また，失語，失行，失認，半側空間無視などの「いわゆる巣症状」が認知症において現れる場合についても紹介する。

Key words

●認知症
●失語
●失行
●失認
●記憶障害

Ⅰ はじめに

認知症とは，認知障害が後天性に起こることによって，社会的・職業的な困難が生じ，病前の機能水準と比べて明らかな低下が起こった病態である。それでは，認知障害とは何かというと，DSM-Ⅳ-TR(Diagnostic and Statistical Manual of Mental Disorders, 4th edition, Text Revision)では，記憶障害，失語，失行，失認，実行機能の障害が挙げられ，ICD-10(International Classification of Diseases, 10th revision)では，記憶，思考，見当識，理解，計算，学習能力，言語，判断を含む多数の高次皮質機能障害と表現されている。DSM-Ⅳの記述は，アルツハイマー病(Alzheimer's disease；AD)の記憶障害と脳卒中における巣症状とを混ぜ合わせた内容であり，古典的な神経心理学が対象としてきた症候の羅列である。ここでは，記憶障害といわゆる巣症状，すなわち認知症を構成する神経心理学的症状とその病巣・メカニズム論について概説する。

Ⅱ 記憶障害

記憶とは，広く「エピソード，知識，行為，手続きのいかんを問わず，あらゆる体験を脳が処理できるかたちに符号化(encode)し，貯蔵(store)し，取り出す(retrieve)機能の総体」と捉えられる[1]。認知症でみられる代表的記憶障害はエピソード記憶障害である。しかし，知識に

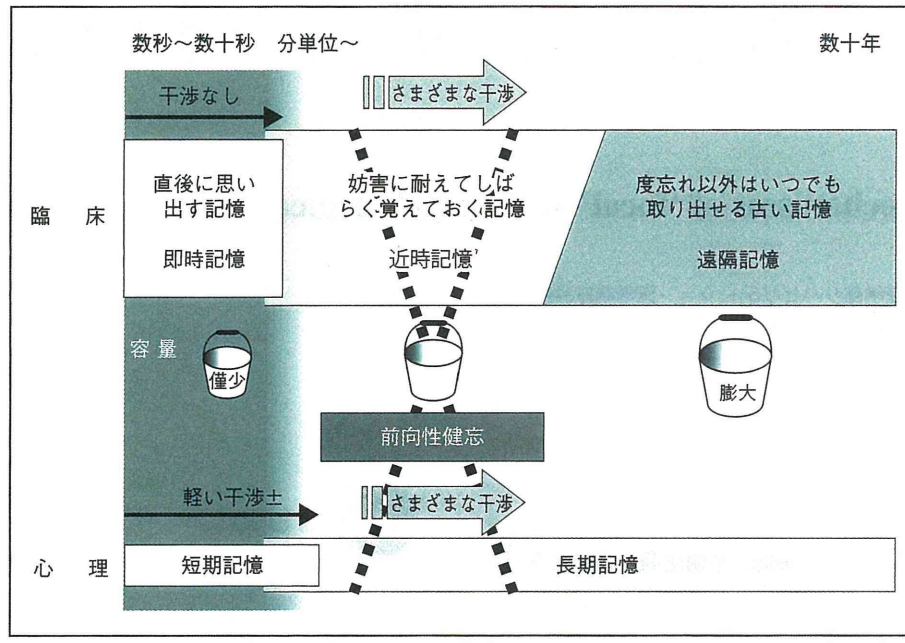

図1　記憶の時間経過による分類

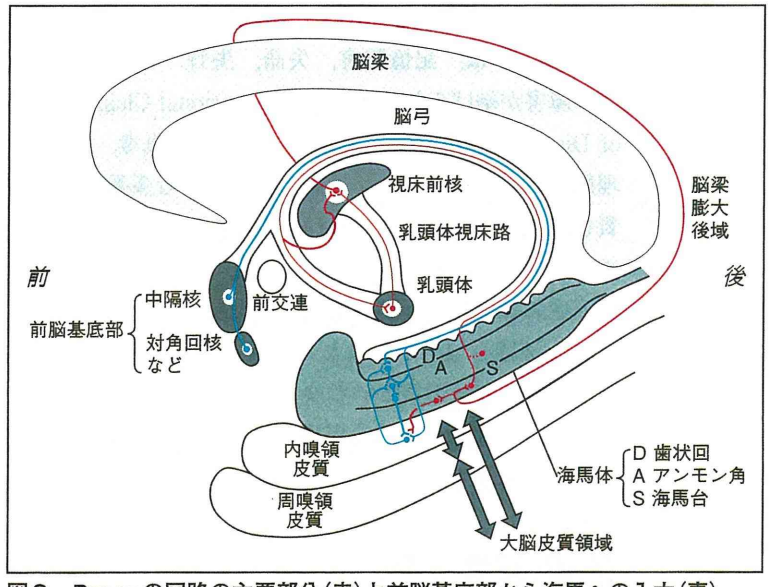

図2　Papezの回路の主要部分(赤)と前脳基底部から海馬への入力(青)
(石合純夫．高次脳機能障害学．医歯薬出版，2003より引用)

近い記憶である意味記憶の障害，また情報の短期間保持・処理ならびにそれらに注意資源を分配する中央遂行系の機能を包括するワーキングメモリーの障害も起こる。

1．時間の流れとエピソード記憶障害

時間の流れを個体の活動において有機的に結び付けているのが記憶である。時間経過に沿った記憶の分類を**図1**に整理した。体験したことを深い処理をしないでそのまま一時的に蓄える記憶が「即時記憶(心理学では，ほぼ短期記憶に相当)」である。次いで，他の情報による干渉に耐えて数分以上覚えておく記憶を「近時記憶(心理学では長期記憶)」という。注意と即時記憶がほぼ保たれているにもかかわらず，干渉刺激のある数分以上をもちこたえられないのが「近時記憶障害」，いわゆる「もの忘れ」である。新たな体験を覚えられないという意味で「前向性健忘」ともいう。この症状は，側頭葉内側部の海馬を中心とするPapezの回路(**図2**)[1]の損傷で起こることが多い。ADでは初期から，話を聞いたり，さまざまな体験をしたりしても，他のことをすればまもなく忘れてしまう。一方，情報量が多くなければ，復唱やその場その場の応答は比較的良好である。すなわ

ち，近時記憶が障害された前向性健忘が主体であり，初期には即時記憶は保たれている。症状が進行すれば，即時記憶の容量も低下してくる。遠隔記憶は，度忘れを除いていつでも取り出せる堅固な記憶である。ADでは遠隔記憶は比較的良好であるが，古い記憶ほど病期が進行しても残りやすい。

2．その他のタイプの記憶障害

時間の流れを伴うエピソードではなく，知識のような記憶を意味記憶という。前頭側頭型認知症(frontotemporal dementia；FTD)[2]のうち意味性認知症(意味型原発性進行性失語)では，初期から意味記憶の障害が起こり，左側頭葉萎縮が目立つ。この場合，皮質領域だけでなく，下縦束を含む白質の損傷の関与が指摘されている[3]。認知症では，記憶の一時的貯蔵や注意配分の切り替えなどワーキングメモリーに相当する機能の障害も起こる。

Ⅲ 失　語

失語とは，語を想起し，適切に選択・配列して意思を表出し，また表現された内容を理解する「言語」の機能が，大脳病変により障害された状態である。右利き者では，大半が左半球損傷後に起こる。

1．認知症における失語

著しく進行した時期を除けば，AD患者と話していて失語という印象を受けることは少ない。少なくとも左大脳半球の脳卒中で生じた典型的な失語症状はみられない。強いていえば，いいたい言葉が出てこない喚語困難が目立つ一方，流暢な発話であるがゆえに，健忘失語の範疇に分類される。しかし，FTDのうち，原発性進行性失語では初期に失語が前景に現れる。その分類と特徴を**表1**に示す[4]。

2．言語の神経ネットワークと失語症状

失語症の診察は，滑らかな流暢性発話か，たどたどしく途切れ途切れな非流暢性発話かという「流暢性」の評価に始まり，言語理解と復唱の成績を加えて，失語型の分類へと進める。失語の古典的タイプ分類を**図3**[1]に示す。認知症では，脳卒中でみられるような典型的分類が難しい場合も少なくないが，変性や萎縮が比較的限局性

表1　原発性進行性失語(primary progressive aphasia)の分類と特徴

	非流暢/失文法型 Nonfluent/agrammatic variant	意味型 Semantic variant	語減少症型 Logopenic variant
	(進行性非流暢失語，progressive nonfluent aphasia)	(意味性認知症，semantic dementia)	
Ⅰ臨床診断	①失文法 ②発語失行を伴う努力性，途切れ途切れの発話 の少なくとも一方がある	①呼称障害 ②単語レベルの理解障害 の両方がある	①自発話と呼称における喚語困難 ②文と句の復唱障害 の両方がある
	①複雑な統語構造をもつ文の理解障害 ②単語レベルの理解は良好 ③物体の知識は保存 のうち2つ以上を満たす	①物体の知識の障害：特に低頻度ないしは熟知性の低いもの ②表層性失読または失書 ③復唱は良好 ④発話は流暢 のうち3つ以上を満たす	①自発話と呼称における音韻性錯語 ②単語レベルの理解が良好，かつ物体の知識が保存 ③運動性発話の保存* ④明らかな失文法がない のうち3つ以上を満たす
Ⅱ画像診断	左前頭葉後部から島に優位の萎縮，血流/代謝低下	側頭葉前部に優位の萎縮，血流/代謝低下	左シルビウス裂後部周辺または頭頂葉に優位の萎縮，血流/代謝低下

*発語失行や構音障害のような発語の運動側面の障害はないが，喚語困難や音韻性錯語による休止があり，速度や量は制限されていてもよい。

に言語領域の一部に生じれば，その部位に応じた失語症状が現れうる。**図4**に言語に関わる神経ネットワークと原発性進行性失語の脳萎縮分布の関係を示す。

Ⅳ 失　行

失行とは，学習された行為を意図的に遂行する能力の障害である[1]。①行為に関する指示の内容を理解し，②道具を使用する場合には対象物の認知が成立し，③運動麻痺，失調，感覚障害など動作を障害する要因がないにもかかわらず，行為をうまく遂行できない。評価としては，「さよなら」や「敬礼」のような象徴的行為と道具使用の身振りを行う。巣症状としては，左半球の頭頂葉または前頭葉の病巣で起こる症状である。

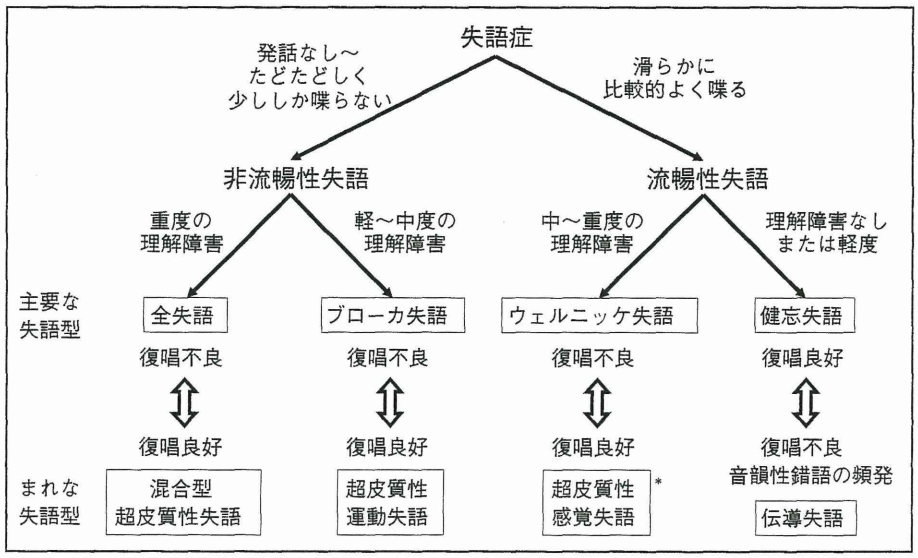

図3　失語型の分類の流れ
*語義失語は，理解障害が語の意味に生じるという特徴があるが，超皮質性感覚失語の1つのタイプといえる。
（石合純夫．高次脳機能障害学．医歯薬出版，2003より引用）

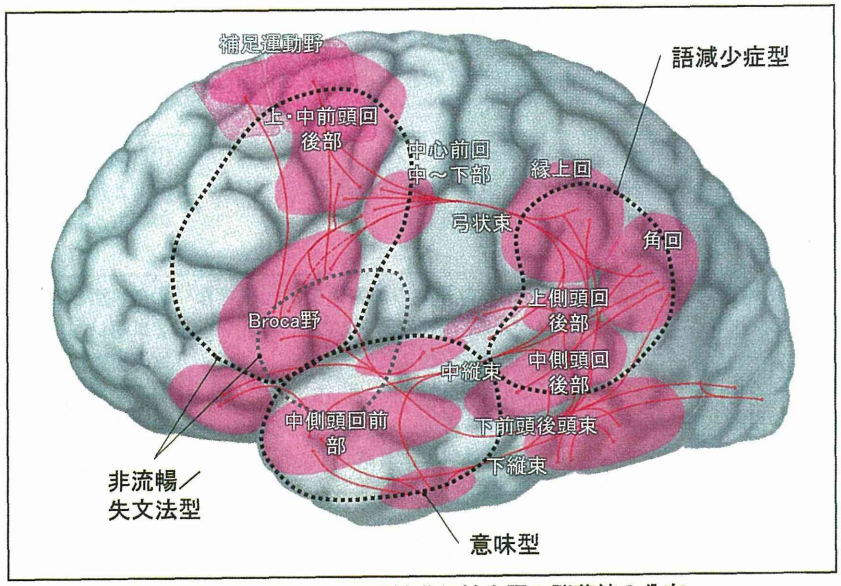

図4　言語の神経ネットワークと原発性進行性失語の脳萎縮の分布